IMSc/2006/03/09

Neutrino oscillation probabilities: Sensitivity to parameters

D. Indumathi, M.V.N. Murthy, G. Rajasekaran and Nita Sinha
The Institute of Mathematical Sciences,
Chennai 600 113, India.

(Dated: February 2, 2008)

Abstract

We study in detail the sensitivity of neutrino oscillation probabilities to the fundamental neutrino parameters and their possible determination through experiments. The first part of the paper is devoted to the broad theme of isolating regions in the neutrino (and anti-neutrino) energy and propagation length that are sensitive to the oscillation parameters. Such a study is relevant to neutrinos both from the Earth's atmosphere or from a neutrino factory. For completeness we discuss the sensitivity, however small, to the parameters involved in a three-generation framework, and to the Earth matter density profile. We then study processes relevant to atmospheric neutrinos which are sensitive to and allow precision measurements of the mixing angle θ_{23} and mass-squared difference δ_{32} apart from the mixing angle θ_{13}. Crucial to this analysis is charge identification; detectors having this capability can isolate these matter effects. In particular, we address the issue of using matter effects to determine whether the mixing angle θ_{23} is maximal, and, if not, to explore how well its octant can be determined. When realistic detector resolutions are included, we find that deviations of about 15% (20%) from a maximal value of $\sin^2\theta_{23} = 1/2$ can be measured at 95% (99%) CL) provided θ_{13} is non-zero, $\sin^2\theta_{13} \geq 0.015$, and the neutrino mass ordering is normal, with fairly large exposures of 1000 kton-years.

PACS numbers: 14.60.Pq, 96.40.Tv, 95.55.Vj

I. INTRODUCTION

Observations of solar, atmospheric, reactor and long-baseline neutrinos have provided compelling evidence for neutrino oscillations [1, 2, 3, 4]. In fact, the latest analysis of the data from the Super-Kamiokande (Super-K) collaboration [5] presents a clear and unambiguous evidence for the oscillation hypothesis [6, 7] by establishing the first *oscillation minimum* and hence for non-zero (and different) neutrino masses and mixing. In the meanwhile, the Sudbury Neutrino Observatory (SNO) [1] has provided incontrovertible evidence for neutrino oscillation from solar neutrino data.

Clearly neutrino physics is now entering an era of precision measurements. The focus from now on will be to precisely determine the oscillation parameters apart from the observation of the oscillation pattern beyond the first minimum. Given the reach of present and proposed experiments, the goal is to understand in detail the sensitivity of the oscillation probabilities to fundamental neutrino parameters, which are the mass-squared differences and mixing angles and phases. It is therefore crucial to choose processes or observables that maximise the sensitivity to the parameter(s) of interest.

It turns out that the density profile of matter that the neutrinos pass through before detection naturally accentuates the sensitivity to the mixing angles θ_{13}, θ_{23} and the mass squared difference δ_{32}. These *matter effects* have been studied before, with atmospheric neutrinos, in various contexts, in Refs. [8, 9, 10, 11, 12, 13, 14, 15, 16]. In particular, substantial matter dependences occur in the energy range of interest only if $\sin^2\theta_{13}$ is different from zero; a non-zero value of this parameter also opens the window to CP violation in the lepton sector. Since only an upper bound exists on this parameter so far, the variation in sensitivity to other parameters can be large or small, depending on the true value of θ_{13}.

This paper is devoted to the detailed study of oscillation probabilities of energetic (GeV energy) neutrinos and anti-neutrinos propagating through the Earth in a three flavour framework using accurate numerical methods. The paper is divided into two parts: The first part is devoted to the broad theme of sensitivity of the neutrino (and anti-neutrino) oscillation probabilities to the fundamental neutrino parameters in the GeV region. The results of this analysis are equally applicable to atmospheric neutrinos as well as to neutrino beams from future neutrino factories. While some of this information is already known, we emphasise a few surprising variations.

Having determined the various sensitivities, we then use the results of the first part to maximise matter effects in a study of atmospheric neutrinos (and anti-neutrinos) using detectors having charge identification capability and study how best these parameters can be constrained/determined by such an analysis.

The paper is organised as follows. In section 2, we outline the framework for the calculation of neutrino probabilities. Though numerical procedures have been developed to calculate any desired survival or conversion probability, in this paper we focus on the probabilities relevant for the accurate calculation of muon-neutrino (and anti-neutrino) events at a detector. We also list here the current limits on the oscillation parameters.

In section 3, we consider, in turn, the variation of the muon neutrino survival and conversion probabilities as the oscillation parameters are varied within the allowed limits. The compendium of results listed here applies generically to any combination of neutrino source and detector where GeV energy neutrinos traverse the Earth.

In section 4, we present results for event rates calculated with atmospheric neutrinos.

We also identify in passing interesting regions in energy–nadir angle space for long-baseline neutrinos. The results are calculated for up/down ratios of event rates binned as a function of the zenith angle or equivalently distance L to bring out the maximal sensitivity to parameters, especially θ_{13}, θ_{23} and the sign of δ_{32}. The question of hierarchy from the sign of δ_{32} has been discussed in detail before [16]; we focus here on the sensitivity of event rates and event ratios to the magnitude of this parameter. An important open question is the deviation from maximal of the mixing angle θ_{23}, that is, its octant sensitivity. This was analysed recently by Choubey and Roy [15]; we present results here which are complementary to their analysis. The issue of both the mass hierarchy and the octant of θ_{23} have relevance to the structure of neutrino mass models.

In section 5 we present a summary of our results and conclusions; we also highlight the improvement over the earlier results. Some remarks on the numerical computation are presented in the appendix. We also discuss the possible points of departure from earlier calculations, especially those that have been used in neutrino event generators such as NUANCE [17].

II. OSCILLATION PROBABILITIES

For completeness we review the basic framework used in evolving the neutrino states and the calculation of oscillation probabilities. In a three neutrino framework, the neutrino flavour states $|\nu_\alpha\rangle$, $\alpha = e, \mu, \tau$, are defined as linear superpositions of the neutrino mass eigenstates $|\nu_i\rangle$, $i = 1, 2, 3$, with masses m_i :

$$|\nu_\alpha\rangle = \sum_i U_{\alpha i} |\nu_i\rangle \ . \tag{1}$$

The $|\nu_\alpha\rangle$ are the states produced in association with the charged leptons. The 3×3 unitary matrix U may be parametrised [7] (ignoring Majorana phases, which may be included by multiplying U by a diagonal phase matrix involving two more phases in addition to δ) as:

$$U = \begin{pmatrix} c_{12}c_{13} & s_{12}c_{13} & s_{13}e^{-i\delta} \\ -c_{23}s_{12} - s_{23}s_{13}c_{12}e^{i\delta} & c_{23}c_{12} - s_{23}s_{13}s_{12}e^{i\delta} & s_{23}c_{13} \\ s_{23}s_{12} - c_{23}s_{13}c_{12}e^{i\delta} & -s_{23}c_{12} - c_{23}s_{13}s_{12}e^{i\delta} & c_{23}c_{13} \end{pmatrix}, \tag{2}$$

where $c_{ij} = \cos\theta_{ij}$, $s_{ij} = \sin\theta_{ij}$ and δ denotes the CP violating (Dirac) phase. The 3×3 neutrino mass matrix M_ν^2 in the charged-lepton mass basis is diagonalised by U:

$$U^\dagger M_\nu^2 U = \mathrm{diag}(m_1^2, m_2^2, m_3^2). \tag{3}$$

The fundamental neutrino parameters therefore are the mixing angles θ_{ij}, phase δ, and the mass-squared differences $\delta_{ij} \equiv m_i^2 - m_j^2$.

The time evolution of the mass eigenstates is governed by the Schroedinger equation,

$$|\nu_i(t)\rangle = e^{-iE_i t} |\nu_i(0)\rangle. \tag{4}$$

Consequently the time evolution of the flavour states is given by the equation,

$$i\frac{\mathrm{d}}{\mathrm{d}t}\left[\nu_\alpha\right] = \frac{1}{2E} U M_\nu^2 U^\dagger \left[\nu_\alpha\right] \ . \tag{5}$$

where $[\nu_\alpha]$ is the vector of flavour eigenstates, $[\nu_\alpha]^T = [|\nu_e\rangle, |\nu_\mu\rangle, |\nu_\tau\rangle]$.

The evolution equation in the presence of matter is given by

$$i\frac{\mathrm{d}}{\mathrm{d}t}\left[\nu_\alpha\right] = \frac{1}{2E}\left[UM_\nu^2U^\dagger + \begin{pmatrix} A & 0 & 0 \\ 0 & 0 & 0 \\ 0 & 0 & 0 \end{pmatrix}\right]\left[\nu_\alpha\right] \ , \tag{6}$$

where the matter term A (ignoring the diagonal neutral current contribution) is given by

$$A = 2\sqrt{2}G_F n_e E = 7.63 \times 10^{-5}\ \mathrm{eV}^2\ \rho(\mathrm{gm/cc})\ E(\mathrm{GeV})\ \mathrm{eV}^2. \tag{7}$$

Here G_F and n_e are the Fermi constant and electron number density in matter and ρ is the matter density. The evolution equation for anti-neutrinos has the sign of A and the phase δ reversed.

In general, the 3-flavour probabilities, in particular, $P_{\mu\mu}$ and $P_{e\mu}$ of interest here, depend on all the oscillation parameters: θ_{12}, θ_{23}, θ_{13}, δ_{21}, δ_{32}, and the CP phase δ. We will focus everywhere on effects due to propagation in (Earth's) matter. It is useful to compute these probabilities in the constant density approximation for comparison with the exact numerical results below. We have [18],

$$\begin{aligned} P^m_{\mu\mu} \ &\approx\ 1 - \sin^4\theta_{23}\sin^2 2\theta^m_{13}\sin^2\Delta^m_{31} \ , \\ &\qquad - \sin^2 2\theta_{23}\ \left[\sin^2\theta^m_{13}\sin^2\Delta^m_{21} + \cos^2\theta^m_{13}\sin^2\Delta^m_{32}\right] \ , \\ P_{e\mu} \ &\approx\ \sin^2\theta_{23}\sin^2 2\theta^m_{13}\ \sin^2\Delta^m_{31} \ , \end{aligned} \tag{8}$$

where terms involving δ_{21} have been ignored [16] and the superscript m refers to mixing angles and mass square differences in matter. The relevant L/E-dependent terms in matter are given by,

$$\begin{aligned} \Delta^m_{21} \ &=\ \frac{1.27\delta_{32}L}{E}\frac{1}{2}\ \left[\frac{\sin 2\theta_{13}}{\sin 2\theta_{13,m}} - 1 - \frac{A}{\delta_{32}}\right] \ , \\ \Delta^m_{32} \ &=\ \frac{1.27\delta_{32}L}{E}\frac{1}{2}\ \left[\frac{\sin 2\theta_{13}}{\sin 2\theta_{13,m}} + 1 + \frac{A}{\delta_{32}}\right] \ , \\ \Delta^m_{31} \ &=\ \frac{1.27\delta_{32}L}{E}\ \left[\frac{\sin 2\theta_{13}}{\sin 2\theta_{13,m}}\right] \ . \end{aligned} \tag{9}$$

Note that for sufficiently large values of A/δ_{32}, all the three scales are of the same order of magnitude including Δ^m_{21} which cannot therefore be neglected.

While θ_{13} is small, its value in matter can be enhanced:

$$\sin 2\theta^m_{13} = \frac{\sin 2\theta_{13}}{\sqrt{(\cos 2\theta_{13} - A/\delta_{32})^2 + (\sin 2\theta_{13})^2}} \ . \tag{10}$$

In particular, $\sin 2\theta^m_{13} = 1$ at resonance, when

$$\delta_{32}\ \cos 2\theta_{13} = A \ . \tag{11}$$

Parameter	Best-fit value
δ_{21}	$7.92\ (1 \pm 0.09) \times 10^{-5}$ eV^2
$\lvert\Delta m^2\rvert$	$2.40\ \left(1^{+0.21}_{-0.26}\right) \times 10^{-3}$ eV^2
$\sin^2\theta_{12}$; $[\theta_{12}]$	$0.314\ \left(1^{+0.18}_{-0.15}\right)$; $[34.1^\circ]$
$\sin^2\theta_{13}$; $[\theta_{13}]$	< 0.032; $[10.3^\circ]$
$\sin^2\theta_{23}$; $[\theta_{23}]$	$0.44\ \left(1^{+0.41}_{-0.22}\right)$; $[41.6^\circ]$

TABLE I: Table showing currently accepted [19] best-fit values of oscillation parameters with 2σ errors. In the case of the mixing angle θ_{13}, a 2σ upper bound is shown.

It is convenient to introduce the scale Δm^2[19] instead of δ_{32}:

$$\Delta m^2 \equiv \delta_{32} + \delta_{21}/2 \ = \ m_3^2 - \frac{1}{2}(m_1^2 + m_2^2),$$

so that a normal or inverted hierarchy is simply indicated by a sign (and not magnitude) change in this parameter.

Data on neutrino oscillations are available from the following experiments:

- A combination of solar neutrino experiments and the KamLAND reactor[1, 3] experiment sets limits on the parameters δ_{21} and θ_{12}; it also establishes the mass ordering $m_2 > m_1$.
- A combination of atmospheric neutrino experiments and the K2K experiment[2, 4] constrains the parameters in the (23) sector: δ_{32} (or Δm^2) and θ_{23}. Note that the sign of this mass-squared difference as well as the deviation of θ_{23} from maximality are not yet determined.
- The reactor neutrino experiment, CHOOZ[3], sets an upper bound on the effective (13) mixing angle using the above parametrisation.
- The CP phase δ is unknown.

A combined analysis of these data [19] places limits on the oscillation parameters as summarised in Table I.

III. SENSITIVITY OF OSCILLATION PROBABILITIES TO PARAMETERS

We now discuss in detail the ν_μ, $\bar{\nu}_\mu$ survival and conversion probabilities as these are of interest here. Note that, in the absence of oscillations, the number of events in the neutrino sector is always a factor of two or more larger than in the case of anti-neutrinos due to the larger neutrino cross-section. We will comment further on its implication in section 4.

The extraction of neutrino parameters to high precision requires the determination of neutrino oscillation probabilities in matter to a high degree of accuracy. Analytically, the effect of non-uniform matter poses a problem, while, in principle, the oscillation probabilities may be computed numerically to the requisite precision. Many, sometimes complicated,

analytical formulae exist for neutrino propagation in vacuum and in matter with either constant or variable density [20, 21, 22, 23, 24, 25, 26].

We use a Runge-Kutta solver to calculate the oscillation probabilities for various energies and nadir angles. Some technical details are given in Appendix A. All results presented in this and the following sections have been obtained using the density profile of the Earth as given by the Preliminary Reference Earth Model (PREM) [27] and numerically evolving the flavour eigenstates through Earth's matter. In particular, the approximate expressions for the probabilities as shown in Eq. 9 are not used.

The matter profile in the PREM model is shown in Fig. 1 as a function of the radius r from the centre of the Earth. The density jumps at inner-outer core and core-mantle transitions are clearly seen. An up-going neutrino with nadir angle θ (shown in the upper x-axis) traverses all density zones of radii larger than the corresponding r shown in the lower x-axis. For $\theta = 33^\circ$, neutrinos graze the core-mantle boundary, while for smaller θ, they traverse the core.

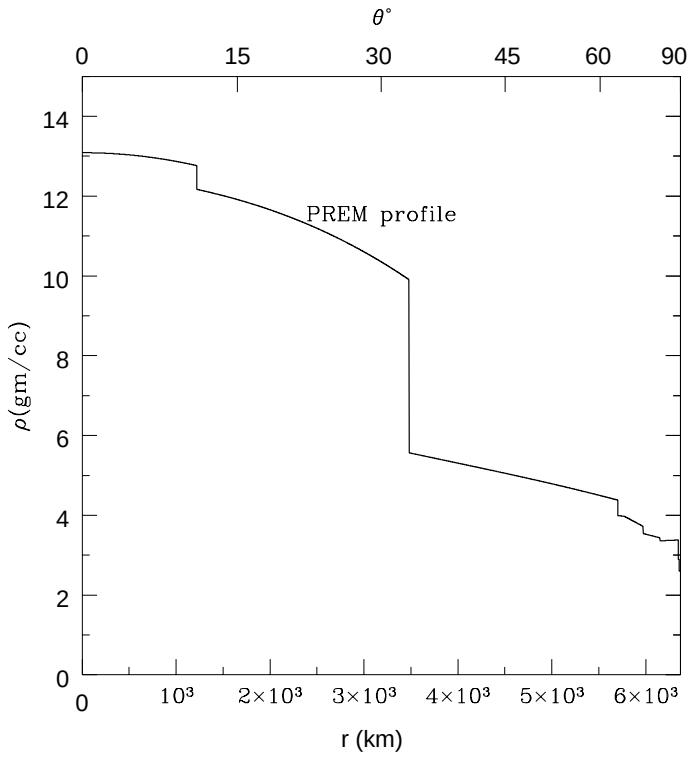

FIG. 1: Variation of the Earth's density profile (assumed spherically symmetrical) with distance from the centre (in km) in the PREM model [27]. The equivalent largest nadir angle of neutrinos that just graze a shell of given radius r is also shown.

We also implicitly assume an iron calorimeter detector with charge identification capability as in the MINOS[29] and the proposed MONOLITH [28] and ICAL/INO [30] detectors. We therefore focus on neutrino energies in the GeV range which is of relevance to these detectors. We will see that the most interesting and sensitive region, purely in terms of the probabilities, is between 2–10 GeV. We look at the sensitivity of the oscillation probabilities to the fundamental neutrino parameters, namely the mass squared differences δ_{21}, Δm^2, the

mixing angles θ_{12}, θ_{13}, θ_{23} and the CP phase δ.

In order to assess the parameter sensitivity, we consider 2σ variations from the current best fit value of each parameter while the others are kept at their best fit values. We shall see that the probabilities are sensitive mainly to the (23) and (13) mixing angles and the larger mass-squared difference Δm^2. When matter effects are turned on the probabilities are also sensitive to the sign of this mass-squared difference. There is also a dependence on the density profile of the Earth. We shall discuss these dependences one by one. Since matter effects are proportional to $\sin\theta_{13}$, which is small, we are looking for sub-leading effects. The main role of matter is to enhance $\sin\theta_{13}$ due to resonance effects. Hence, when we emphasise a large effect, it is understood to be "large" with respect to this small parameter; matter effects, unfortunately, remain rather small with respect to the total events/processes we consider and hence need large exposures for their study.

We shall consider neutrino energies in the range 2–10 GeV, which are relevant for atmospheric neutrino studies. Typically, we shall hold other parameters at their known central values when we discuss the variation with any one parameter. In particular, there is only a marginal/negligible dependence of these probabilities on θ_{12} and δm^2_{21} and we shall not discuss them further.

In general the normal hierarchy is assumed; this means that all matter effects are enhanced due to resonance in the neutrino sector, with smaller effects (and no resonances) in the anti-neutrino sector. Since we are only discussing probabilities, there is an approximate symmetry between particle probabilities with normal hierarchy and anti-particle probabilities with inverted hierarchy [16]. This symmetry is exact in the limit that terms containing δ_{21} can be ignored. Thus we choose Δm^2 to be positive (normal hierarchy) while discussing probabilities. Results with the inverted hierarchy are discussed in the next section.

A. Variation of probabilities with θ_{13}

In general, matter effects are significant provided θ_{13} is not small. The dependence of matter effects on this parameter has been exhaustively studied elsewhere [8, 9, 10, 11, 12, 13, 14, 15, 16] and will not be discussed in any detail in this paper. We merely show a sample dependence on this parameter in Figs. 2 and 3 where $P_{\mu\mu}$ and $P_{e\mu}$ are plotted as a function of the nadir angle θ for three energies, $E = 2, 5, 10$ GeV. The variation in the probabilities as θ_{13} varies over its 2σ allowed region, $\theta_{13} < 10.3^\circ$, is significant at small nadir angles for low energies ($E < 3$ GeV), at virtually all nadir angles at larger energies (around $E \sim 5$ GeV), and tapers off at larger energies (by about $E \sim 10$ GeV) when matter effects become irrelevant. Notice the effect of core crossing at nadir angle $\theta = 33^\circ$ which is especially visible when $E = 5$ GeV when $\theta_{13} \neq 0$. .

For completeness we show the relatively weaker sensitivity to this parameter of the anti-neutrino probability $\overline{P}_{\mu\mu}$ in Fig. 4. When the hierarchy is inverted the behaviour of P and $\overline{P}$ are interchanged.

B. Variation of probabilities with Δm^2

We begin with $P_{\mu\mu}$, which is extremely sensitive to this parameter, as can be seen in Fig. 5. The figure shows the variation of $P_{\mu\mu}$ with the nadir angle θ at different neutrino

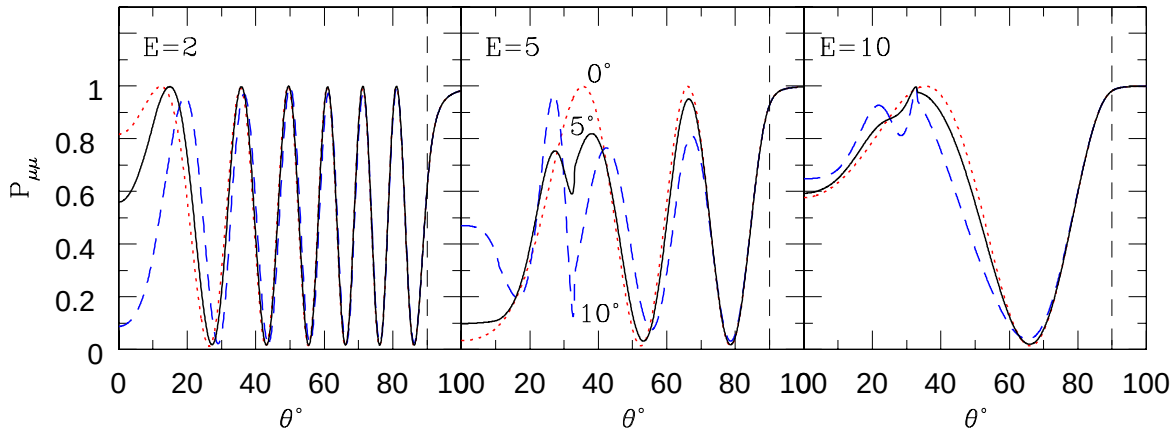

FIG. 2: Variation of $P_{\mu\mu}$ with θ_{13} as a function of nadir angle θ. Probabilities for $\theta_{13} = 0, 5, 10^\circ$ are shown as dotted, solid and dashed lines respectively. Sensitivity to θ_{13} at three different neutrino energies, $E = 2, 5, 10$ GeV, is shown in the three panels. Other parameters are set to their best-fit central values (see Table I). Normal hierarchy is assumed.

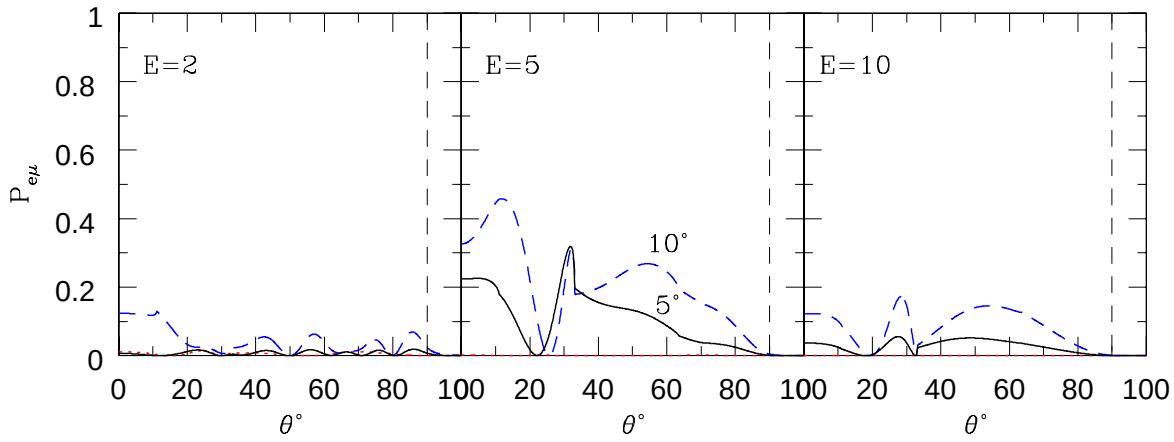

FIG. 3: Variation of $P_{e\mu}$ with θ_{13}. See caption of Fig. 2. Although $P_{e\mu}$ is non-zero when $\theta_{13} = 0$, the non-zero contribution comes from an oscillatory term dependent on δ_{21} and is very small/invisible beyond $E \sim 1$ GeV.

energies, for a 2σ variation of Δm^2: $\Delta m^2 = (1.8, 2.4, 2.9) \times 10^{-3}$ eV^2. The top three panels are for $\theta_{13} = 9^\circ$ and the lower three for $\theta_{13} = 0$ at three different energies. Notice that the smooth oscillations seen in the lower panels are modified due to matter effects (turned on when $\theta_{13} \neq 0$) in the upper panel.

In general, the modification is significant in the small nadir angle bins for lower energies ($E = 2$ GeV), and at all nadir angle bins in the intermediate energy region (represented by the central panel at $E = 5$ GeV) when resonance occurs in the mantle. The interplay between the variation in Δm^2 (even at the 2σ level) and that in the relatively unknown θ_{13} is clear from the $E = 5$ GeV panels: the same muon survival probability for upward-going neutrinos ($\theta = 0^\circ$) can come from $(\Delta m^2, \theta_{13})$ both large: $(2.9 \times 10^{-3}$ eV$^2, 9^\circ)$ or both small: $(1.8 \times 10^{-3}$ eV^2, $\sim 0^\circ)$.

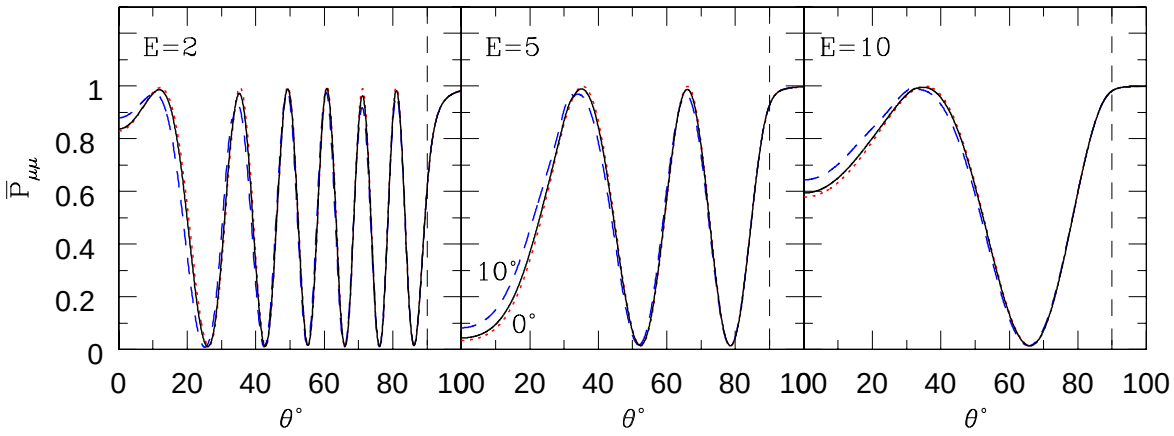

FIG. 4: Variation of $\overline{P}_{\mu\mu}$ with θ_{13}. See caption of Fig. 2.

Since matter effects are relatively unimportant for anti-neutrinos (in the normal hierarchy) the anti-neutrino survival probability at all allowed θ_{13} is close to the neutrino survival probability at $\theta_{13} = 0$. This can be seen from Fig. 6 where $\overline{P}_{\mu\mu}$ is shown. In fact, the difference between the neutrino and anti-neutrino survival probabilities is a measure of the matter effect and hence that of θ_{13} and the sign of Δm^2 (the mass hierarchy) as has been discussed earlier [16].

The conversion probability $P_{e\mu}$ is small unless θ_{13} is substantial. We show the high sensitivity of this probability to variations in Δm^2 for $\theta_{13} = 9^\circ$ in Fig. 7. An interesting feature is the substantially larger probability for small nadir angles (0–30°) and low energy ($E = 2$ GeV) for the $\Delta m^2 = 1.8 \times 10^{-3}$ eV^2 value due to resonance inside the core. This feature is visible only at low Δm^2 values: for example, for $E = 2$ GeV, it occurs roughly for $\delta_{32} \sim \Delta m^2 \lesssim 2.0 \times 10^{-3}$ eV^2, with a small uncertainty in the limit due to the unknown θ_{13}. For larger values of Δm^2, larger densities than are available inside the Earth are needed to satisfy the resonance condition, Eq. 11, at $E = 2$ GeV; hence there is no substantial enhancement of these probabilities in the small nadir-angle region.

A substantial ($> 20\%$) $P_{e\mu}$ in this region at small energies around $E = 2$ GeV is thus a clear indication that $\Delta m^2 < 2 \times 10^{-3}$ eV^2. While this fact may not have an impact on the overall event rates for atmospheric neutrinos, it will be important for long baseline neutrinos since one can separately study $P_{e\mu}$ through *wrong sign muons*. The anti-neutrino conversion probability, however, remains small even for large θ_{13} and is therefore not shown.

C. Variation of probabilities with θ_{23}

The Super-Kamiokande data favour a best-fit value of $\theta_{23} = 45^\circ$ in a 2-flavour analysis. Although a recent 3-flavour global analysis [19] indicates that this parameter may be slightly smaller, $\theta_{23} = 41.6^\circ$, the 2σ allowed parameter space spans both octants: $36^\circ \leq \theta_{23} \leq 52^\circ$. The dominant (matter-independent) term in the survival probability depends on $\sin^2 2\theta_{23}$. It is therefore difficult to substantially decrease errors on θ_{23} via a measurement of the leading contribution. Furthermore, even if a deviation from the maximal value is measured, it is impossible to determine the octant with such a term.

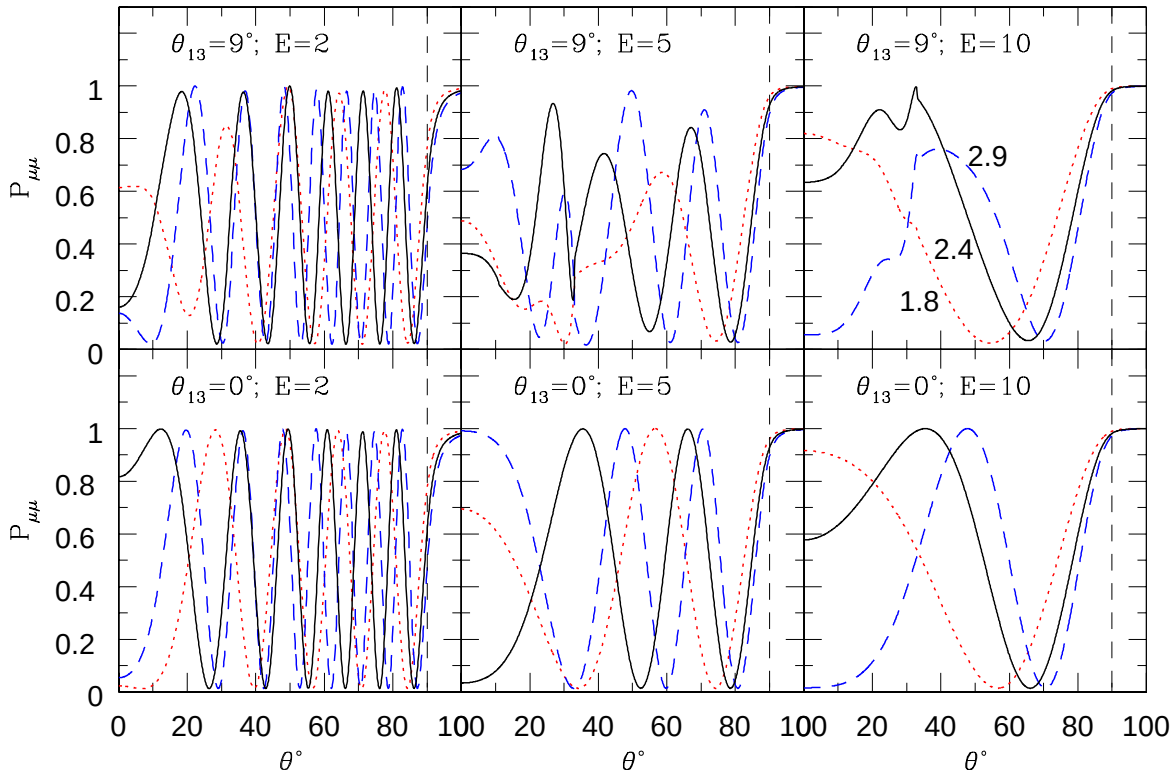

FIG. 5: Variation of $P_{\mu\mu}$ with Δm^2 at $\theta_{13} = 9°$ (upper panels) and $\theta_{13} = 0$ (lower panels). Δm^2 values used are the 2σ allowed variation (dotted line for 1.8×10^{-3} and dashed line for 2.9×10^{-3} eV^2) of this parameter around the solid curve for the best-fit value ($= 2.4 \times 10^{-3}$ eV^2). The values of Δm^2 in units of 10^{-3} eV^2 are marked in the top right panel of the figure.

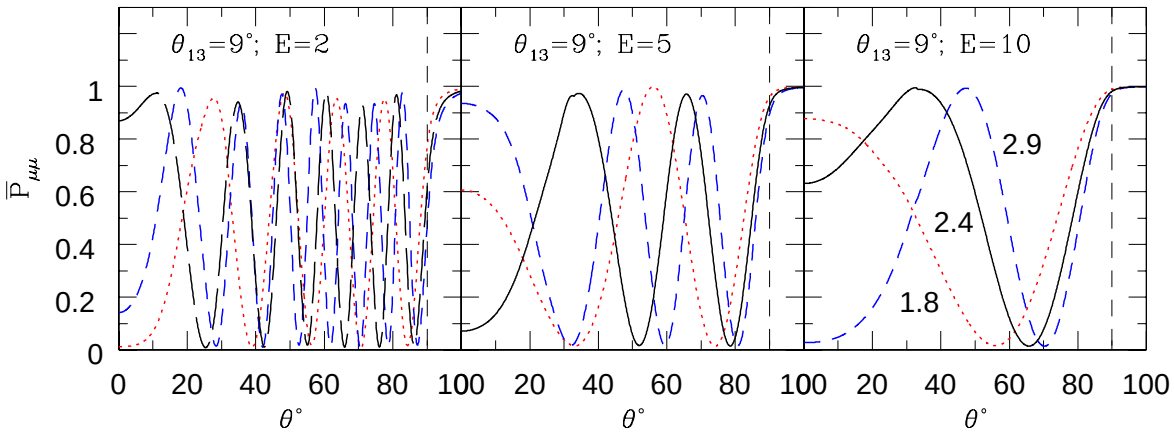

FIG. 6: Variation of $\overline{P}_{\mu\mu}$ with Δm^2 at $\theta_{13} = 9°$. See caption of Fig. 5 for details. The probability is not significantly different at other values of θ_{13} and is similar to the neutrino survival probability in Fig. 5 for $\theta_{13} = 0$.

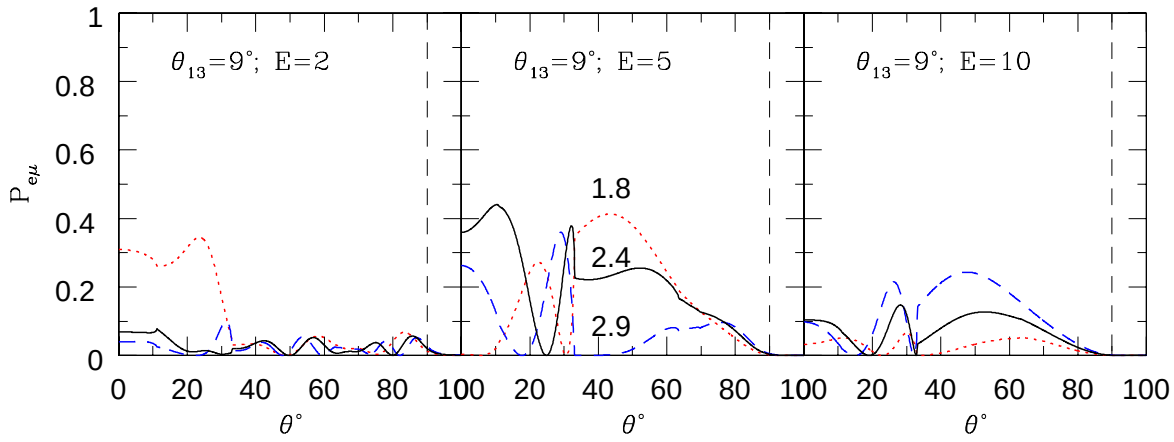

FIG. 7: Variations of $P_{e\mu}$ with Δm^2 at $\theta_{13} = 9°$. See the caption to Fig. 5 for details.

Methods to determine the octant of θ_{23} have been discussed in detail elsewhere [15]. Sensitivity to the octant of this angle is realised through sub-leading terms that depend on θ_{23}, not $2\theta_{23}$, as can be seen from Eq. 9. These are matter-dependent and sub-leading because they are also proportional to $\sin\theta_{13}$, which is known to be small but is otherwise unknown.

Fig. 8 shows the sensitivity of $P_{\mu\mu}$ to variations in θ_{23}. For clarity of discussion, we choose a central value of 45° (that is, choose a maximal value rather than the slightly smaller central best-fit value as used earlier) and the *same* 2σ variation about it. When $\theta_{13} = 0$, symmetric 2σ variations about the central value of 45° lead to the *same* survival probability, as can be seen at all neutrino energies in the lower panels of the figure.

When θ_{13} is not zero, the survival probability for θ_{23} less than maximal (red dotted line) lies consistently above the central value (solid line) for all values of Δm^2, E and nadir angles. This happens because the terms in $P_{\mu\mu}$ involving $\sin\theta_{23}$ and $\sin 2\theta_{23}$ come with the same relative (negative) sign, as seen from Eq. 9. As θ_{23} increases from the first octant towards maximal, both these terms are increasing so that the probability systematically decreases. However, as θ_{23} increases from the maximal to a value in the second octant, $\sin\theta_{23}$ increases while $\sin 2\theta_{23}$ *decreases*, leading to a complicated dependence of the probability on this parameter. Hence no such regular behaviour is seen when θ_{23} is larger than 45° although, in a large portion of phase space at E = 5–10 GeV, the probability for $\theta_{23} < (>)$ 45° is systematically larger (smaller) than that at $\theta_{23} = 45°$.

It is clear from Fig. 8 that, for non-zero θ_{13}, the probability curve for θ_{23} in the first octant (37°) is better separated from that for $\theta_{23} = 45°$, than the curve for θ_{23} in the second octant (53°). Evidently, the ability to determine whether θ_{23} is different from maximal will depend on which octant the true value of θ_{23} lies in. This is also reflected in our numerical results with atmospheric neutrino events, as discussed in the next section.

Precisely the opposite effect is seen in the conversion probability $P_{e\mu}$ as seen in Fig. 9. Here, the probability increases with θ_{23} for all Δm^2 values at all energies and nadir angles so that the probability for $\theta_{23} < (>)$ 45° is *systematically larger (smaller) than the probability with* $\theta_{23} = 45°$. This can be easily seen from the fact that there is a single term proportional to $\sin\theta_{23}$ in Eq. 9 for $P_{e\mu}$, appearing with the opposite sign to the matter terms in $P_{\mu\mu}$. Hence a long base-line experiment, where ν_e and ν_μ beams are separately available, will be

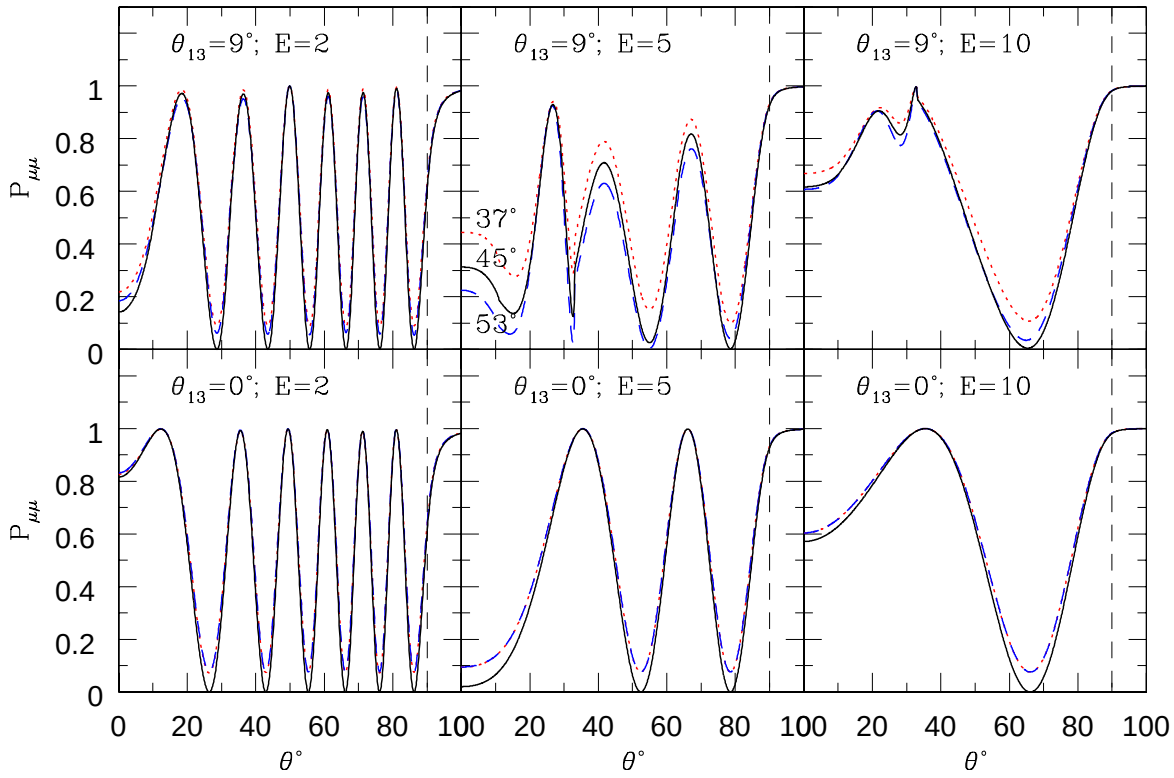

FIG. 8: Variation of $P_{\mu\mu}$ with θ_{23} for $\theta_{13} = 0, 9°$, as a function of the nadir angle. While probability curves for θ_{23} values symmetrically larger and smaller than 45° coincide when $\theta_{13} = 0$ (bottom panels), they differ for non-zero θ_{13} as shown in the top panels.

able to clearly establish the octant of θ_{23} by studying the $P_{e\mu}$ conversion probability via the wrong-sign muon events.

Note that if $\theta_{13} = 0$ exactly, then the octant determination cannot be made from $P_{\mu\mu}$ although $P_{e\mu}$ still shows the same dependence on θ_{23} as discussed above. However, $P_{e\mu}$ is insignificant in this energy range and hence octant discrimination at $\theta_{13} = 0$ is possible only through a study of $P_{e\mu}$ at low energies around 0.1 GeV, when resonance effects in the (12) sector enhance this probability. This is outside the scope of the present paper and will be discussed in a separate publication.

This relatively systematic dependence on θ_{23} is in contrast to the rather complex dependence of the survival and conversion probabilities on Δm^2 and θ_{13}. Both these probabilities contribute to the observed muon events in studies of atmospheric neutrinos. We shall explore this further in a later section to maximise this "octant-seeking" effect.

In contrast, the matter dependence is small for the anti-neutrinos; hence, the anti-neutrino survival probabilities for all θ_{13} values are similar to the neutrino survival probability at $\theta_{13} = 0$ and do not distinguish the octant of θ_{23}. We reiterate that this is a consequence of the chosen hierarchy; opposite results are obtained with the inverted hierarchy (matter effects are ultimately larger in the normal hierarchy since the anti-neutrino cross-sections are smaller than the neutrino cross-sections so that event rates are larger and matter effects better differentiated in the neutrino sector).

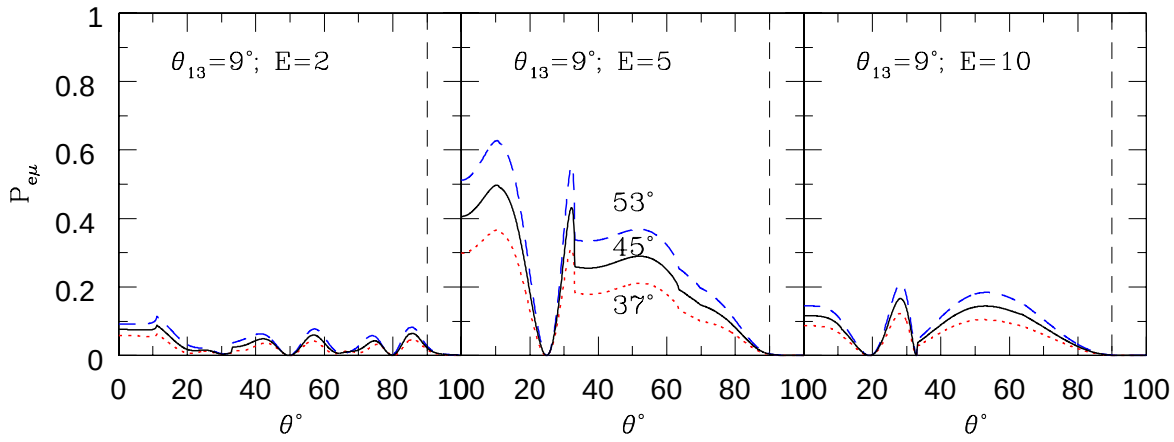

FIG. 9: Variation of $P_{e\mu}$ with θ_{23} for $\theta_{13} = 9°$.

D. Variation of the probabilities with Earth density

In order to compute the effect of Earth's matter on the probabilities, we have used the PREM model [27] which gives the density profile of a "spherical equivalent Earth". While the locations of the discontinuities and mantle-core transitions are rather well-known, the absolute values of the densities themselves are not so well established. Hence, in order to study effects of uncertainties in the Earth's density, we have retained the locations of the discontinuities while changing the density values. We have done this in a simple manner by changing all the densities within the core by $\Delta\rho_{\rm core} = 0.6$ gm/cc (a change of roughly 5%, as allowed by the model), and suitably adjusting the mantle densities in such a way as to maintain the overall mass of the Earth to be constant. Such a procedure results in a much smaller change in the mantle densities of $\Delta\rho_{\rm mantle} \sim -0.2\Delta\rho_{\rm core}$, in the opposite direction.

The consequences of such a density change to the neutrino survival and conversion probabilities are shown in Figs. 10 and 11 respectively. Here $\rho_>$ and $\rho_<$ correspond to increasing and decreasing the core densities by 5%, with the mantle densities adjusted suitably. The solid black line is for the original PREM density profile. Again, the size of matter effects depends on Δm^2; changing the density alters the Δm^2 at which resonance occurs, for a given neutrino energy.

A point to note is the difference between the PREM profile and constant density slabs. The former has a continuously changing density profile, even within slabs. Hence neutrinos with a band of energy can undergo resonance in any given slab. In contrast, only a neutrino with a single definite energy can undergo resonance in a constant density slab (apart from having purely adiabatic propagation inside any slab). Due to this, the probability curve as a function of zenith angle for a given energy can look very different when computed with the PREM profile and with a constant density approximation, even when the latter closely follows the PREM profile. However, when an integration over an energy bin is performed, such variations get averaged out. More details on this issue are given in the Appendix.

At low energies where the matter effects are significant only for core-crossing neutrinos at small nadir angles, the effects of altering the density profile are also seen only at these small nadir angles, as can be seen from the upper panels of the figures. At higher energies, changes appear at larger nadir angles as well, as can be seen from the lower panels, since

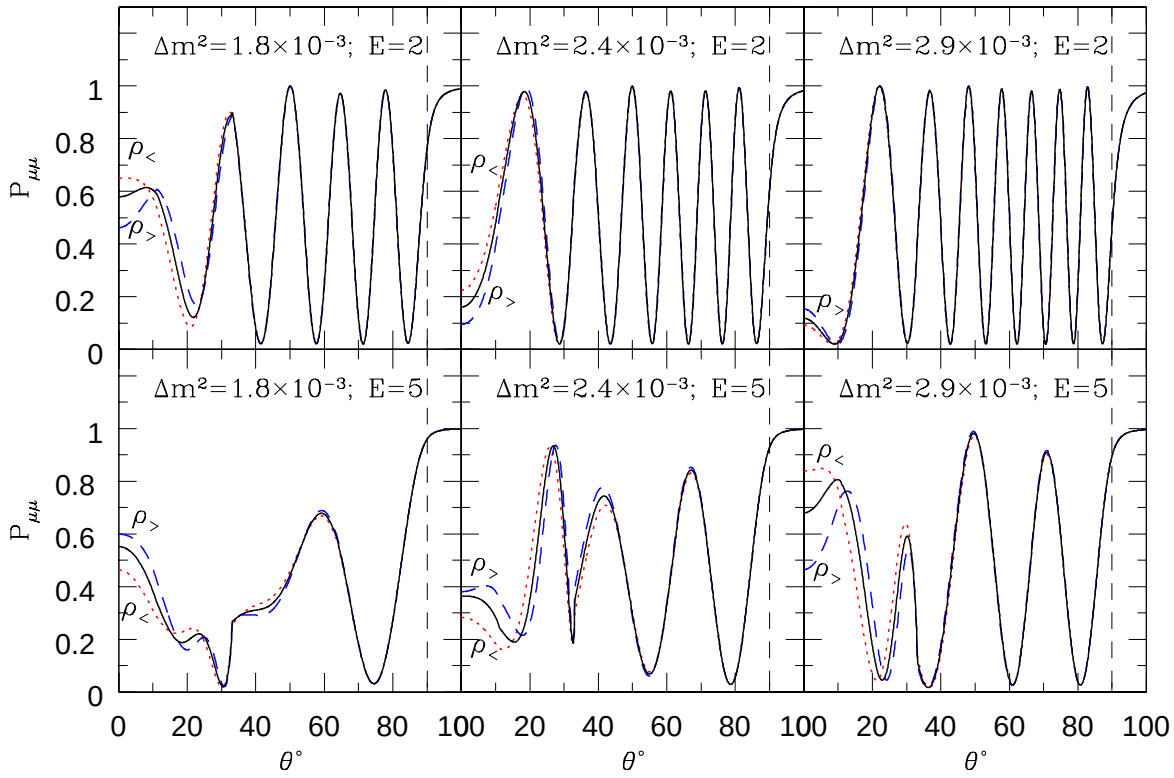

FIG. 10: Variation of $P_{\mu\mu}$ with changes in the Earth's density for $\theta_{13} = 9°$ and a 2σ variation in Δm^2 at $E = 2, 5$ GeV. The curves labelled $\rho_>$ and $\rho_<$ correspond to increasing and decreasing the core densities by roughly 5% (with a compensating change in the mantle densities) compared to the black solid line for the PREM density profile.

resonance (and enhanced matter effects) occurs in the mantle itself. While the variations are small, except at small nadir angles, again, they are complex and depend on both energy and a precise knowledge of Δm^2. Probing the Earth density, especially in the core, with neutrino oscillation physics using neutrino factory beams has been discussed earlier [31]. Here, only the dependence on θ_{13} was considered while Δm^2 was kept fixed.

We remark that in all cases there is also a dependence on θ_{13} at small nadir angles since the variations with θ_{13} are substantial here, as can be seen from Fig. 2. The dependence on density variations may be disentangled from that on θ_{13} since substantial variations in the intermediate nadir angle region can only be due to θ_{13}, as seen from Fig. 2.

The anti-neutrino probabilities again do not show any significant dependence on these parameters in the normal hierarchy.

E. Variation of probability with the CP phase

We now explore the dependence of the probabilities on the CP phase δ. This dependence is shown in Fig. 12, again for $\theta_{13} = 9°$. Apart from the dashed vertical line at $\theta = 90°$ that separates the "up-going" probability from the "down-going" one, the dotted vertical line at $\theta \sim 55°$ indicates the nadir angle corresponding to the so-called "magic base-line" [32] where

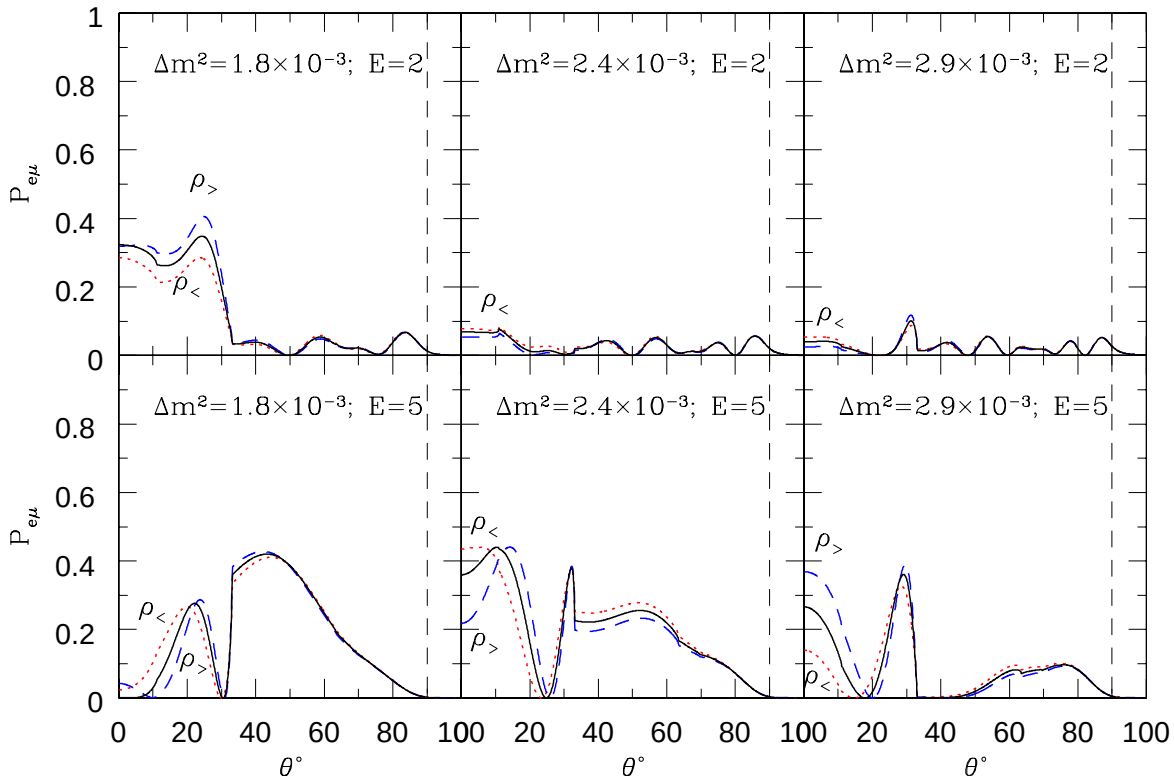

FIG. 11: As in Fig. 10 for $P_{e\mu}$.

the probabilities are independent of the CP phase. Since the Earth mantle density is not a constant, this is actually a band around that nadir angle, as can be seen from the figure.

The effect of the CP phase δ competes with the matter effect which in turn depends on the relative size of the matter term A compared to Δm^2. The variation of the probabilities (as a function of energy and nadir angle) with δ for the current 2σ allowed range of Δm^2 is shown in Fig. 12. This variation is so small that it is unlikely to be measured via a study of atmospheric neutrinos and may need long base-line measurements where the spectrum and nadir angle are well-known. Nevertheless, we make a few remarks on the general behaviour.

While the survival probability $P_{\mu\mu}$ is symmetric for $\delta = \pm\pi, \pm\pi/2$, $P_{e\mu}$ can distinguish the cases $\delta = \pm\pi/2$. At low energy, $E = 2$ GeV, the top panels in Fig. 12 indicate that the survival probability $P_{\mu\mu}$ is typically larger for $\delta = 0$ at all nadir angles, smaller for $\delta = \pm\pi/2$ and smallest for $\delta = \pm\pi$, *independent* of Δm^2. This is not true at larger energies, as can be seen from the lower panels of the figure. Hence, if these small variations can indeed be measured, information on δ may be obtained with some confidence, only if Δm^2 is known to much better than the current precision.

The situation is murkier with the conversion probability $P_{e\mu}$, as can be seen from Fig. 13. The clear trend that was visible with $P_{\mu\mu}$ at low energy is no longer present. At $E = 5$ GeV there is a systematic trend between the curves for $\delta = 0$ and $\pi/2$ and between $\delta = -\pi/2$ and $\pm\pi$; they behave in the same way relative to each other. The complex effect of δ is overlaid on an already small $P_{e\mu}$. Signatures of $P_{e\mu}$ are very clean however with long-baseline detectors (via wrong-sign muon measurements); this may facilitate a measurement of δ at such detectors, as has been discussed elsewhere [33].

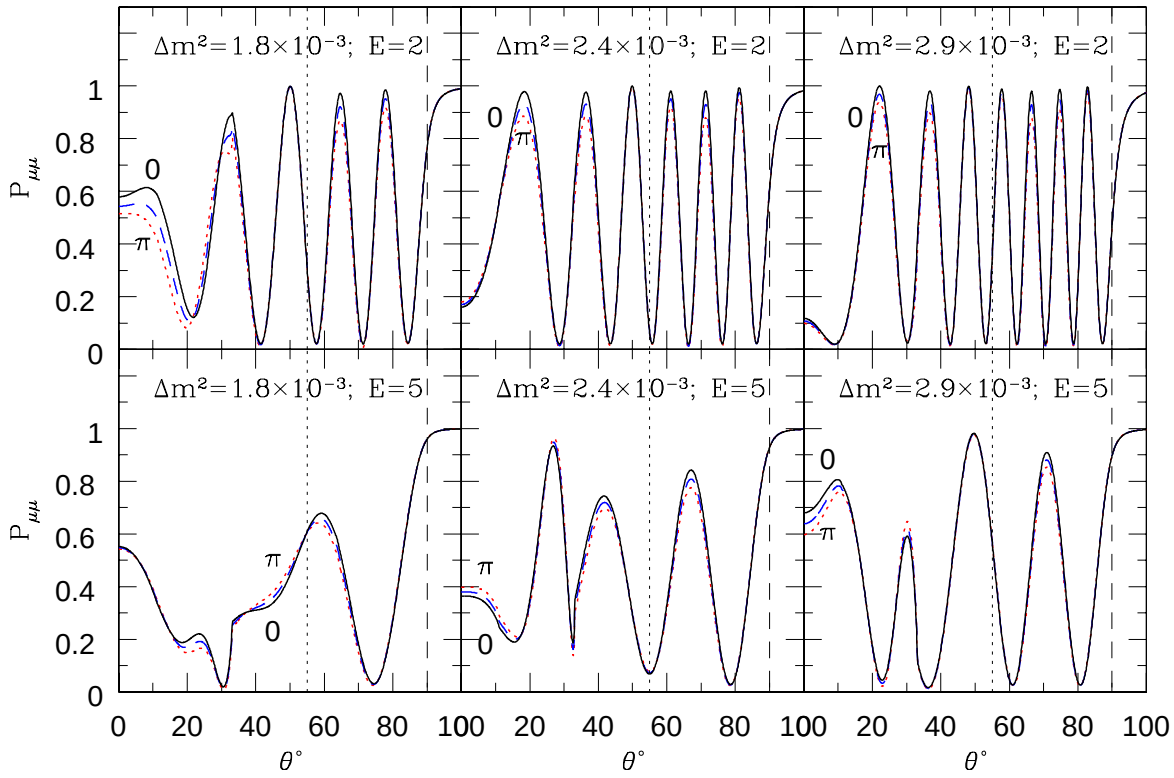

FIG. 12: Variation of $P_{\mu\mu}$ as a function of nadir angle with the CP phase δ for $\theta_{13} = 9°$, for a 2σ variation of Δm^2. The curves shown are for $\delta = 0, \pm\pi/2$, and $\pm\pi$. The vertical dotted line indicates the magic base-line where the probabilities are independent of δ.

The anti-neutrino probabilities are rather insensitive to matter effects or the CP phase (in the normal hierarchy) and we do not discuss them here.

IV. EVENT RATES IN A DETECTOR

A. Preliminaries

While one can identify clearly the regions of sensitivity to the fundamental neutrino parameters through an analysis of the oscillation probabilities, it is crucial to identify the appropriate observables which will enable a precision measurement of the parameters. The experimental observables are primarily the event rates in a detector. The fully differential event rate for neutrinos of flavour α to be detected is given by the general expression:

$$\frac{\mathrm{d}N^\alpha}{\mathrm{d}E\mathrm{d}x} = K_y \sum_\beta \Phi_\beta(E,x)\ P_{\beta\alpha}(E,x)\ \sigma_\alpha(E)\ , \tag{12}$$

where $x = L/E$ and σ_α is the total interaction cross-section for the α type neutrino to interact with the detector material. Here $P_{\beta\alpha}$ is the conversion probability of a neutrino of flavour β to a flavour α (which also includes the survival probability when $\alpha = \beta$).

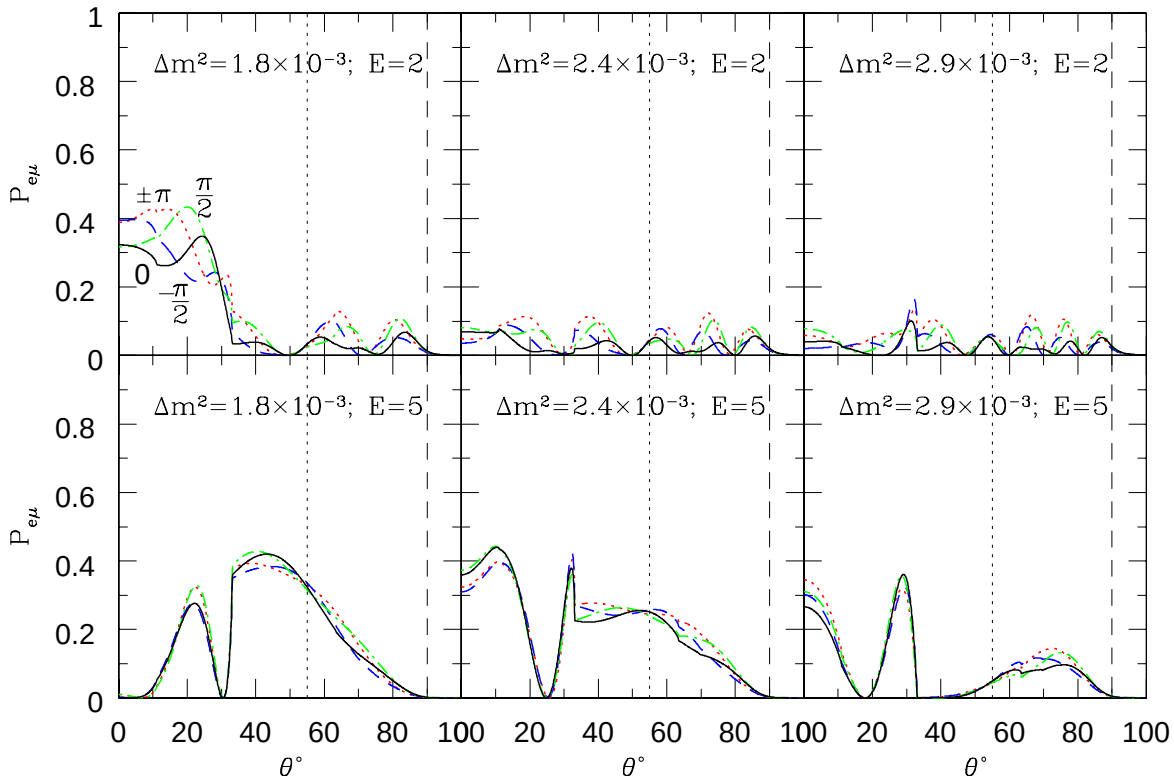

FIG. 13: As in Fig. 12 for $P_{e\mu}$. The curves shown are for $\delta = 0, \pi/2, -\pi/2$, and $\pm\pi$.

The flux-dependent term $\Phi_\beta(E, x)$ is related to the doubly-differential neutrino (or anti-neutrino) flux of flavour β, $\mathrm{d}^2\phi_\beta(E,\theta)/\mathrm{d}\ln E\,\mathrm{d}\cos\theta$, which is a function of the energy E and nadir angle θ through a Jacobean of transformation. In the case of atmospheric neutrinos a range of zenith angles are available while for long-baseline neutrinos this angle is kept fixed by the location of the source.

The factor K_y is the detector dependent factor measured in units of kton-years. While we assume the detector to be mainly made up of magnetised iron with active detector elements, this is not crucial since only the detector mass and exposure times are relevant. In the MONOLITH and ICAL/INO proposals, where muons from charged-current ν_μ-nucleus interactions are detected, the active detector elements are resistive plate chambers (RPCs, gas-filled glass chambers). In either of these proposals the detector mass is almost entirely ($> 98\%$) due to its iron content. We will be interested here in *event ratios*; hence the factor K_y and other actual detector details will only determine the errors. Furthermore, we assume that the detector is capable of correctly identifying the charge of the muons in the final state. This will be better than 98% for energies $2 \leq E \leq 10$ GeV for the ICAL/INO detector. This is crucial for the precision determination of the neutrino parameters in any future experiment.

B. Atmospheric Neutrinos

We now focus on neutrino oscillation studies with atmospheric neutrinos. Both ν_μ and ν_e (and their anti-particles) are produced, typically in the ratio 2:1.

The distance of propagation L of the neutrino from the point of production to the detector is given by,

$$L = \sqrt{(R_0 + L_0)^2 - (R\sin\theta)^2} + R\cos\theta \ , \tag{13}$$

where L_0 is the average height (taken to be 15 km) above the surface of the Earth at which the atmospheric neutrinos are produced, R_0 is the radius of the Earth and $R = R_0 - d$, d being the depth at which the detector is located underground (chosen to be 1 km). Note that $\theta = 0$ corresponds to neutrinos reaching the detector vertically upwards.

The event rate in a given bin of $x = L/E$ is,

$$N^{\alpha}_{\rm bin}(x) = \int_{\rm bin} {\rm d}x \int_{E_{\rm min}} \frac{{\rm d}E}{E} \frac{{\rm d}^2 N^{\alpha}}{{\rm d}\ln E {\rm d}x} \ ; \tag{14}$$

henceforth we discuss only the case of muon-neutrinos, $\alpha = \mu$ (or $\overline{\mu}$). Then both $P_{e\mu}$ and $P_{\mu\mu}$ contribute in the expression above. However, due to the smallness of the (13) mixing angle, θ_{13}, the contribution of $P_{e\mu}$ is generally small and is significant only near large L/E where it is about 10–20% (5%) for neutrinos (anti-neutrinos).

The event rate is expressed as a function of x, averaged over a bin width that will be appropriately chosen to maximise the sensitivity to the sign of δ_{32} or the octant of θ_{23}. The expression given in Eq. 14 is the best-case scenario since the integration is over the neutrino or anti-neutrino energy. We discuss the effect of including the detector resolution functions in the next section and proceed now to analyse the ideal case with a perfect detector.

C. Event rates with an ideal detector

A useful measure of oscillations is the ratio of up-coming to down-going neutrinos with nadir/zenith angles interchanged. This is clear from Fig. 14. The fluxes of atmospheric neutrinos from directions θ and $(\pi-\theta)$ are expected to be similar in the absence of oscillations, especially for larger energies (E greater than a few GeV). Since the path-length traversed, L, is related to θ as

$$L = f(|\cos\theta|) + R\cos\theta \ ,$$

(see Eq. 13), the replacement $\theta \leftrightarrow (\pi - \theta)$ effectively changes the sign of the second term in the equation above, thus taking, for instance, a down-going neutrino to an up-coming one. The ratio of events in the up-down directions for a given $x = L/E$, therefore, reflects the asymmetry of the up-down fluxes, due to oscillations. We define [34],

$$\mathcal{R} = \frac{U}{D}(x) = \frac{\text{No. of events from up-coming muon neutrinos}(x)}{\text{No. of events from down-going muon neutrinos}(\tilde{x})} \ ,$$

where $\tilde{x} = x(\theta \leftrightarrow (\pi - \theta))$ and the number of up-coming (U) or down-going (D) events is calculated using Eq. 14. Similarly the ratio $\overline{U}/\overline{D}$ defines the corresponding up/down ratio for anti-neutrinos. Since the effect of oscillations on the denominator is small, the ratio $\mathcal{R}$ is effectively the ratio of oscillated to unoscillated events with the same L/E.

While reflecting the effect of oscillations, this ratio also minimises errors due to the uncertainties in the overall flux normalisation (which can be as large as 30%) and those in the cross-sections (about 10%). We now proceed to determine these ratios numerically, and study their sensitivity to the oscillation parameters of interest.

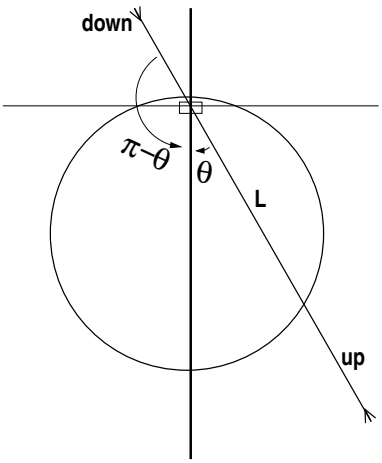

FIG. 14: A schematic showing the up- and down- neutrino directions and their labelling in the nadir angle θ.

We use the 3D atmospheric neutrino fluxes as calculated by Honda et al. [35]. These have been obtained from the NUANCE neutrino generator [17]. The charged current muon-neutrino nucleus cross-sections used have also been extracted from the NUANCE code. At the low end of the energy spectrum, the interaction with the detector material is mainly through quasi-elastic and resonance interactions. When the energy is a few GeV, deep inelastic scattering (DIS) dominates, ultimately taking over by about 10 GeV, as this cross-section is proportional to the neutrino energy. There are still issues about the transition from the resonance (mainly single pion dominated) region to the DIS region [17]; however, such errors are minimised by *always analysing ratios of events*. Roughly speaking, in the energy range of interest from few to 10's of GeV, half the events are from quasi-elastic and resonance interactions and the other half from DIS. This proportion is somewhat sensitive to finite detector resolutions, since the neutrino energy is smeared over a much larger range than that observed; however, the events are still dominantly low-energy ones owing to the steep fall (faster than $1/E^2$) of the incident atmospheric neutrino flux with energy.

We find, as studies of the probabilities suggest, that variations of the event rates due to uncertainties in δ_{21} and θ_{12} are small. We therefore fix them to their best-fit values. We also set the CP phase $\delta = 0$ and fix the Earth's density to be as given by the PREM density profile [27]. The remaining parameters, viz., Δm^2 (both magnitude and sign), θ_{13} and θ_{23} (in particular, its deviation from maximality and hence also its octant), are the parameters to be determined or constrained in the analysis. A study of atmospheric neutrino events is sensitive to all these parameters (but the magnitude of Δm^2) only through matter effects. That is, θ_{13} must be non-zero and substantial for there to be any sensitivity to these parameters. Since this parameter is known to be small, it therefore follows that large exposures are required to determine any of the above parameters to better precision than are currently known.

In order to proceed further, we shall assume in the following that θ_{13} is substantial; the precise threshold will be determined through the analysis. It is already known that the sign of Δm^2 can be determined via the *difference asymmetry* of the up/down ratios in the neutrino and anti-neutrino channels:

$$\mathcal{A} = U/D - \overline{U}/\overline{D} \ , \tag{15}$$

where U and D are the relevant differential event rates for up and down events as a function of L/E and $\overline{U}$ and $\overline{D}$ the corresponding rates for anti-neutrinos. This asymmetry can be maximised by choosing to integrate over L/E bins that include one half-period of the oscillation. This can be approximated by the matter-independent condition,

$$\frac{1.267|\delta_{32}|L}{E} = n\frac{\pi}{4}\ ; \quad n \text{ odd.} \tag{16}$$

A detailed analysis of this asymmetry has already been done in Ref. [16]; we only remark here that we require $\sin^2 2\theta_{13} \geq 0.06$ ($\theta_{13} \geq 7^\circ$) for the sign of Δm^2 to be determined using this technique. Furthermore, this determination requires 750–1000 kton-year exposure, depending on the value of θ_{13}, thus setting the scale for our present analysis.

We focus therefore on the precision to which the magnitude of Δm^2 and the octant of θ_{23} can be determined, given such large exposures. (Current data from the Super-Kamiokande collaboration restrict these to the ranges $1.8 \leq |\Delta m^2| \times 10^3$ eV$^2 \leq 2.9$ and $36.5 \leq \theta_{23} \leq 54.5^\circ$.) This again depends on $\sin^2\theta_{13}$, which is expected to be shortly measured with good precision (to within a few percent) by the Double-CHOOZ experiment [36]. We study both cases: when θ_{13} is known and hence kept fixed in the analysis, as well as the case when it is allowed to vary freely. We restrict ourselves to the normal hierarchy, with Δm^2 positive, so that matter effects (and hence sensitivity to the octant of θ_{23}), are enhanced in the neutrino channel. We integrate event rates over an energy range of E = 5–10 GeV to maximise statistics while retaining sensitivity to matter effects.

In Fig. 15 we show the variation of the up/down events ratio for different Δm^2 values as a function of $\log_{10} L/E$ for two values of $\theta_{23} = 40^\circ, 50^\circ$, in two octants. Here θ_{13} is fixed to 9°. Two features are immediately noticeable: (1) the position of the minima and maxima in L/E are not altered by changing θ_{23}; furthermore, the events ratio at the first minimum is not very sensitive to θ_{23}, and (2) the effect of changing θ_{23} from a value in the first octant to a corresponding one in the second octant is to systematically *decrease the event rates in all bins* for all Δm^2 values.

Furthermore, although not shown in the figure due to constraints of clarity, the curve for maximal $\theta_{23} = 45^\circ$ lies between the two curves for $\theta_{23} = 40, 50^\circ$ in all L/E bins beyond the first minimum. Such a systematic decrease with increase in θ_{23} was seen only in some zenith angle and energy ranges (for example for θ = 0–70° for E = 5 GeV and for θ = 0–50° for E = 10 GeV, when $\theta_{13} = 9^\circ$; see the top panels of Fig. 8). By a judicious choice of the energy and L/E interval, this effect has been converted to a systematic difference for all bins to the right of the first minimum; moreover, it is in these bins that the sensitivity to θ_{23} is significant, so that this dependence is robust and easy to observe.

Note that the difference asymmetry defined in Eq. 15 is a difference between neutrino and anti-neutrino rates ratios. In this case, the systematic decrease with increasing θ_{23} is true in *all* L/E bins for any Δm^2 value, by definition. That is, the result for $\theta_{23} = 45^\circ$ always lies between that for a value of θ_{23} in the first and second octant. This is shown in Fig. 16. However, as can be seen from the relative size of the error bars, the task of actually extracting the octant of θ_{23} from measurement of such an asymmetry is severely limited by statistics. In fact, it is the poor statistics in the anti-neutrino sector that limits the efficacy of this parameter.

The effect of increasing θ_{13} away from zero is seen in Fig. 17 where the events ratio is plotted as a function of $\log_{10} L/E$ for different Δm^2 values. The two histograms for each

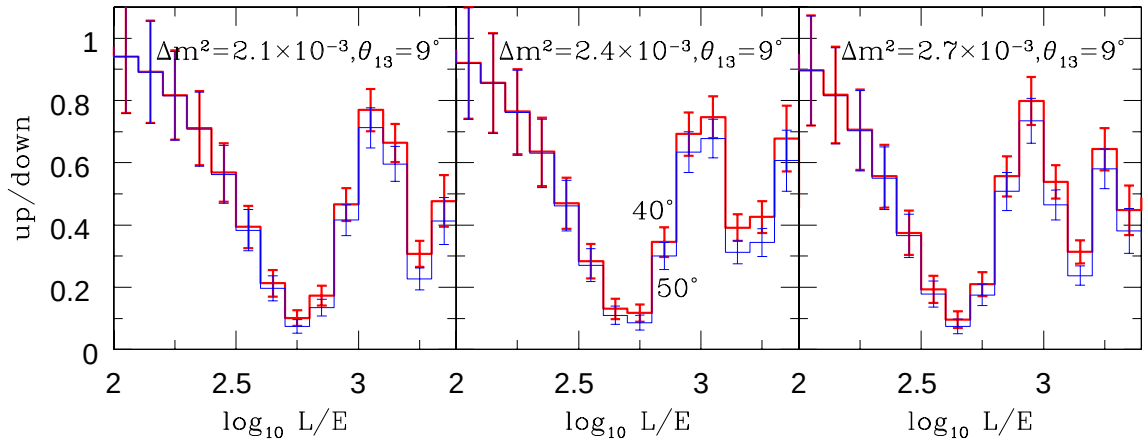

FIG. 15: Variation of the ratio of the rates for up-coming and down-going neutrinos, integrated from $E = 5$–10 GeV, in bins of $\log_{10} L$ (km)$/E$ (GeV) $= 0.1$. The variation with Δm^2 is shown in the three panels, where results for a Δm^2 over the currently allowed 1σ range, via., $\Delta m^2 = (2.1, 2.4, 2.7) \times 10^{-3}$ eV^2 are shown. The two histograms in each panel correspond to $\theta_{23} = 40°$ (upper) and $50°$ (lower). The value of θ_{13} is kept fixed at $9°$. Statistical error bars corresponding to an exposure of 1000 kton-years are also shown.

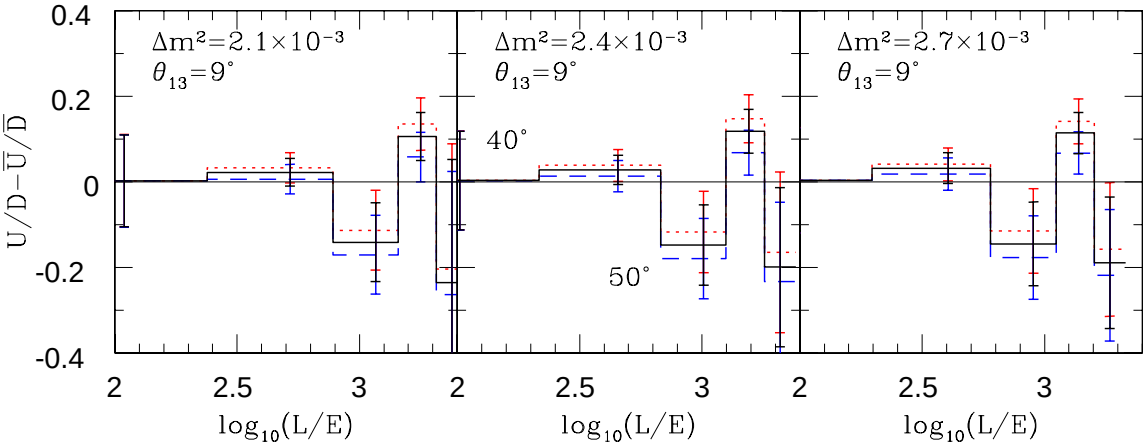

FIG. 16: As in Fig. 15, but for the difference asymmetry, $A = U/D - \overline{U}/\overline{D}$. Three histograms are shown, for $\theta_{23} = 40°$ (dotted), $45°$ (solid) and $50°$ (dashed lines), as a function of $\log_{10} L/E$ in bins defined in Eq. 16. It is seen that the histograms for $\theta_{23} < 45°$ and $\theta_{23} > 45°$ are systematically greater and less than that for $\theta_{23} = 45°$.

Δm^2 value correspond to $\theta_{13} = 0, 9°$, where the latter value is simply chosen as being within the range allowed by current data and where matter effects are known to be substantial. The effect of increasing θ_{13} is to turn on matter effects that move the muon survival probability maxima (as a function of $\log_{10} L/E$) away from 1 and the minima away from zero. This means that for non-zero θ_{13} the events ratio is smaller at probability maxima and larger at probability minima than for $\theta_{13} = 0$. (Note that the extent of deviation is somewhat suppressed by the sub-dominant contribution of $P_{e\mu}$ to the dominant $P_{\mu\mu}$ terms; experiments

such as those with neutrino factories where such contamination does not exist will be even more sensitive to matter effects).

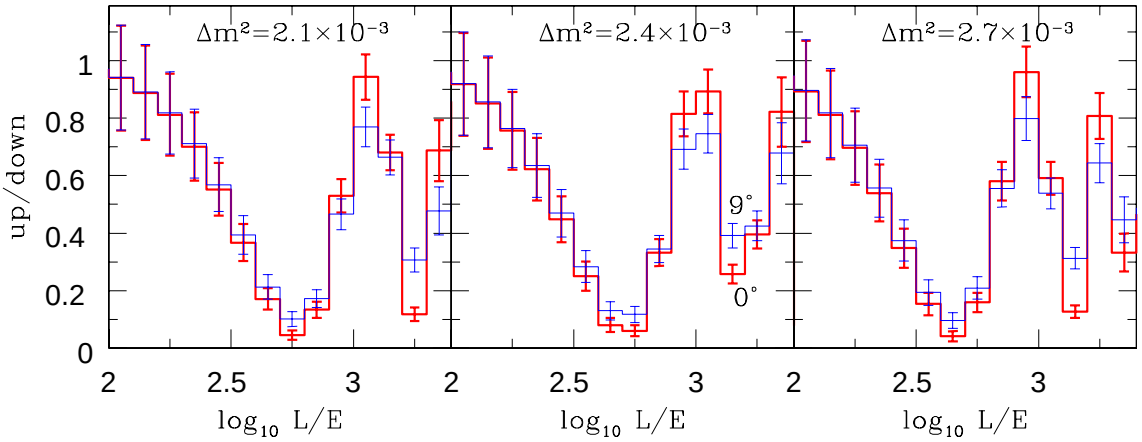

FIG. 17: As in Fig. 15, but for fixed $\theta_{23} = 40°$, while $\theta_{13} = 0, 9°$ in each panel. The outer histogram (larger at maximum and smaller at minimum) corresponds to $\theta_{13} = 0$.

The contrasting behaviour of the events up/down ratio with θ_{13} and θ_{23} for a given Δm^2 is clear: an increase in the latter systematically decreases the ratio, while an increase in the former decreases the ratio at the $\log_{10} L/E$ maxima and increases them at the $\log_{10} L/E$ minima. Such behaviour enables the extraction of the different parameters when the data is fitted to the theory.

To demonstrate this (and to determine the efficacy and precision with which the parameters can be determined), we begin by computing up/down neutrino events ratios for the set of input parameters, $(\theta_{13}, \theta_{23}, \Delta m^2) = (7°, 40°, 2.4 \times 10^{-3}\ \text{eV}^2)$, in different $\log_{10} L/E(\text{km/GeV})$ bins from 1.6 to 3.4 of width 0.1 each. We then fit this "data" to these three parameters, and extract the allowed parameter space to establish how well these parameters can be determined. In particular, we focus on the precision of measurement of all parameters as well as the possible determination of the octant of θ_{23}. Since we are considering ratios, we include only statistical errors in our analysis. Note that a zenith angle cut on very horizontal events that may not be easily detected by horizontally aligned detectors such as ICAL/INO only removes the small L/E bins. For instance, a cut of $\cos\theta = 0.1$ leads to a cut on $\log_{10} L/E \geq 2.15$. For such small values, as can be seen from Fig. 17, there is negligible dependence of the up/down ratio on the neutrino oscillation parameters. Hence, such cuts will not affect our analysis.

Fig. 18 shows the allowed region at 95% CL and 99% CL in the $(\theta_{13}, \theta_{23})$ parameter space, using standard χ^2 minimisation, for a fixed value of $\Delta m^2 = 2.4 \times 10^{-3}$ eV^2. At 95% CL, the up/down ratio barely disallows maximal mixing in θ_{23}; it also disallows the "wrong" octant solution of $\theta_{23} = (\pi/2 - \theta_{23}^{\text{input}}) = 50°$. However, both these sensitivities go away at the 99% CL level when an island of allowed parameter space opens up around the wrong-octant solution, in a region to the right of it.

At this point we note that θ_{13} is likely to be rather precisely fixed (to much better than a percent) by the Double-CHOOZ experiment [36]. We therefore observe the effect of keeping θ_{13} fixed and varying the other two parameters. This is shown in Fig. 19 where the allowed

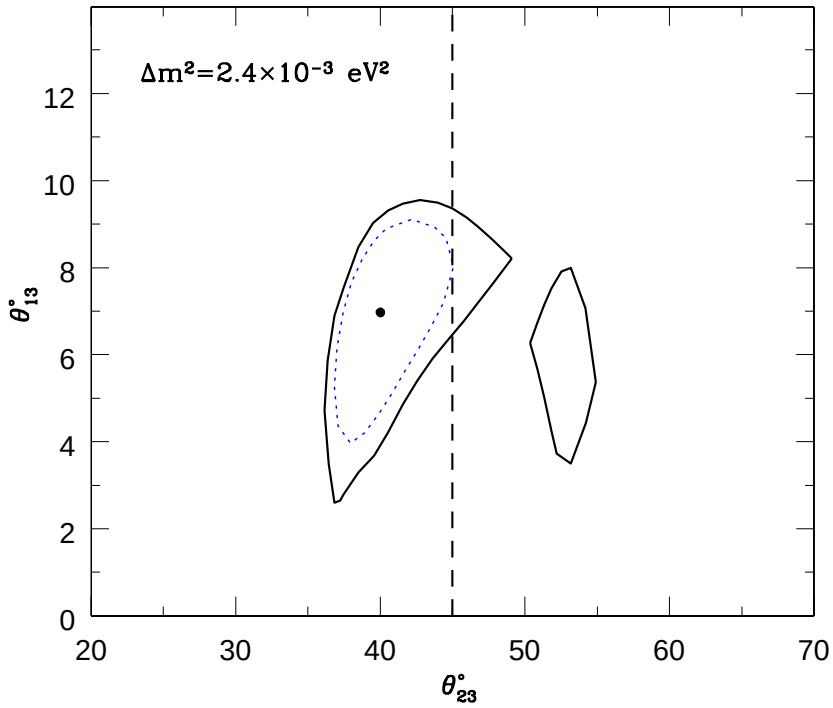

FIG. 18: Allowed parameter space in (θ_{23},θ_{13}) variables. Input used was $(40°, 7°)$, for $\Delta m^2 = 2.4 \times 10^{-3}$ eV^2 (shown as the solid point, also the best-fit). Shown are the 95% and 99% CL contours; it is seen that the "wrong-octant" solution to the right of $\theta_{23} = 50°$ is allowed at 99% CL.

parameter space in $(\theta_{23}, \Delta m^2)$ space is shown for the same input parameters as before. Again, both the maximal solution and the wrong octant solution for θ_{23} are disallowed at 95% CL level. While maximality is still disallowed, a small island opens up around the wrong-octant solution at the 99% CL, again to the right of it. Also, Δm^2 is constrained to a precision of better than 6% at 3σ.

The results are a complicated function of both θ_{13} and Δm^2. In general, the wrong-octant and maximal solution is disallowed at 95% CL up to an input value of $\theta_{23} = 42°$ or $48°$, i.e., a deviation of $3°$ away from maximal in either direction (or 10% deviation in $\sin^2\theta_{23}$) but is allowed at 99% CL. This result is mildly dependent on the value of θ_{13} with results obviously improving for larger θ_{13}. For instance, the 99% CL contours for the same input data set are plotted in Fig. 20 for $\theta_{13} = 7°, 9°$. The precision in Δm^2 is marginally worse for the larger θ_{13}; however, although at both values of θ_{13} maximality is disallowed at 99% CL, the wrong-octant solution is completely disallowed only for the larger (13) mixing angle.

It is possible to reduce the allowed parameter space by adding the contribution of the anti-neutrinos as well. That is, we now consider the input "data set" to consist of both the neutrino and anti-neutrino events ratios. Since we always consider up/down ratios to minimise errors due to overall normalisation of fluxes and cross-sections, this still means that we need to separate the charged muons with good efficiency (that is, identify the process as originating from a neutrino or anti-neutrino). In principle, charge misidentification can lead to systematic errors since, for example, a neutrino event wrongly identified not only is lost from its parent sample, but also adds to the anti-neutrino events. However, in proposed

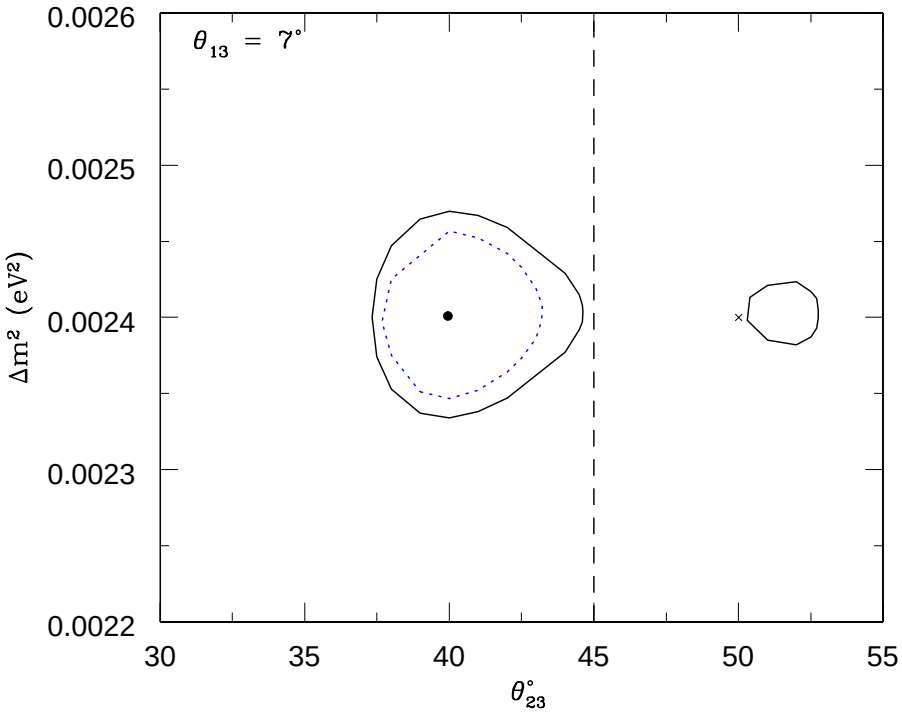

FIG. 19: Allowed parameter space in $(\theta_{23}, \Delta m^2)$ variables. Input used was neutrino up/down event rates at $(40°, 2.4 \times 10^{-3}$ eV$^2)$, for $\theta_{13} = 7°$. Shown are the 95% and 99% CL contours.

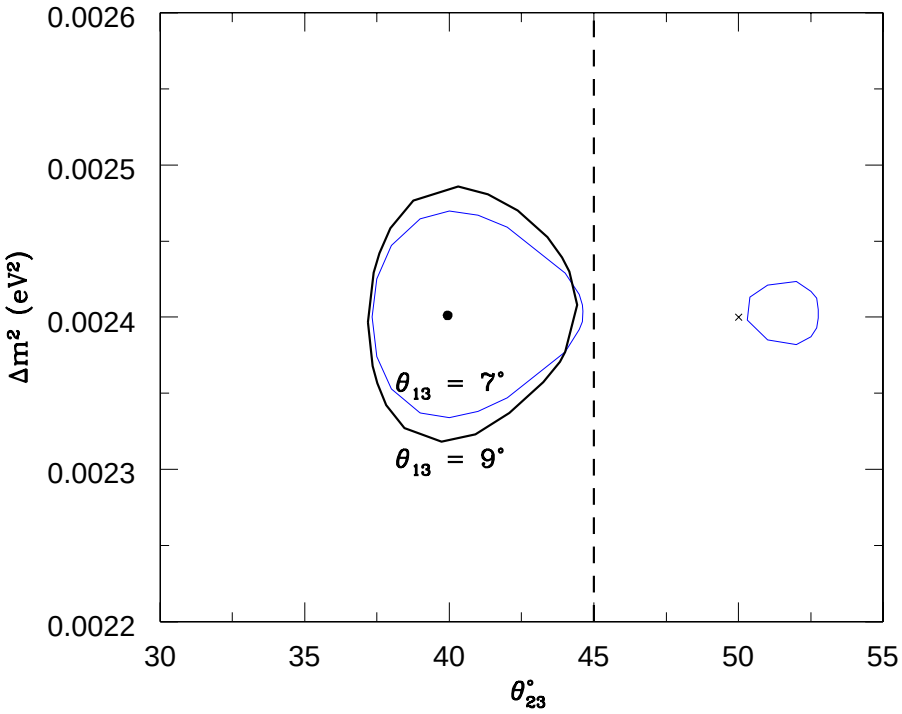

FIG. 20: As in Fig. 19, but for different θ_{13} values. Shown are the 99% CL contours for $\theta_{13} = 7°, 9°$.

experiments such as ICAL/INO, charge identification efficiency in this energy range is better than 98% so we ignore such correlation errors.

We show the allowed parameter space on including both the neutrino and anti-neutrino data sample in Fig. 21. Here the complex dependence on the input value of Δm^2 is also shown: as Δm^2 is increased between its current 1σ allowed values of $\Delta m^2 \sim (2.1\text{–}2.7) \times 10^{-3}$ eV^2, the allowed parameter space in $(\theta_{23}, \Delta m^2)$ around the wrong-octant solution shrinks, and disappears at the upper value of Δm^2. Hence, it appears that deviations from maximality as well as determination of the octant can be typically easily established at the 95% CL level, provided θ_{13} is well-known (and at least of the order $\theta_{13} = 7^\circ$). Results at the 99% CL level are harder to quantify and reflect the complex nature of this many-parameter problem.

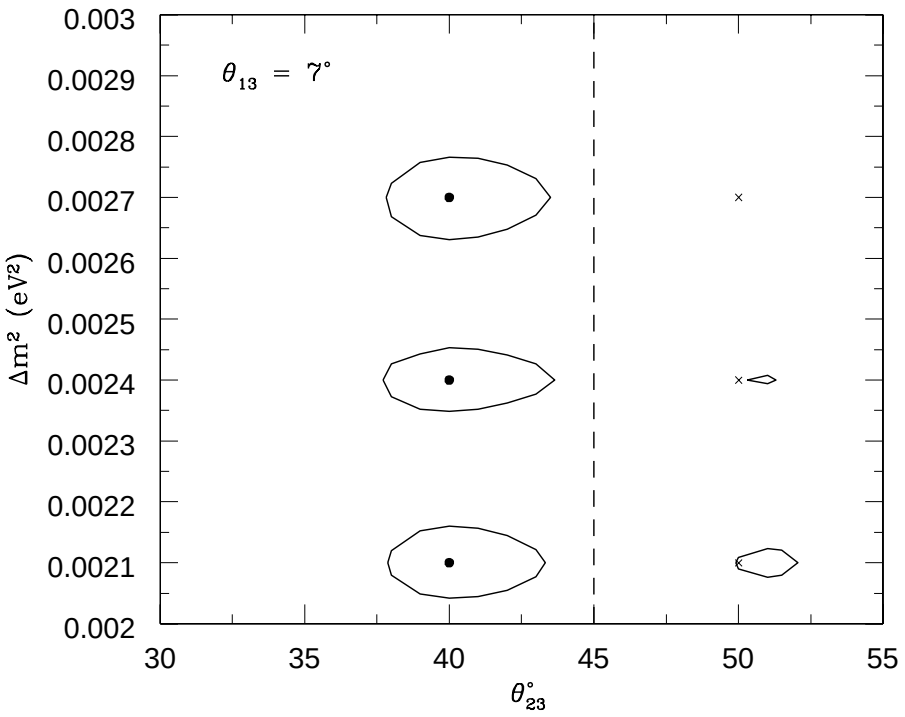

FIG. 21: As in Fig. 19, for the sum of neutrino and anti-neutrino up/down event rates, for $(\theta_{23}, \theta_{13}) = (40^\circ, 7^\circ)$ but for a 1σ variation in Δm^2 of $\Delta m^2 = (2.1, 2.4, 2.7) \times 10^{-3}$ eV^2. While the wrong-octant solution, that is, the region around $\theta_{23} = 50^\circ$ is disallowed at 95% CL in all cases (not shown in the figure), it is allowed at the 99% CL level as shown. Deviation from maximality can always be established at 99% CL.

We now ask how sensitive these results are to the finite resolution (in determining neutrino energy and direction, and hence its L/E) of the detector.

D. Event rates with finite detector resolution

Inclusion of finite detector resolution reduces the sensitivity, especially beyond the first oscillation minimum and maximum in L/E. The smearing in direction affects the resolution in path-length. A straightforward way to include such effects is to smear the observed energy

and direction of the neutrino with Gaussian resolution functions:

$$R_1(E', E) \equiv \frac{1}{\sqrt{2\pi}\sigma_E} \exp\left[\frac{-(E-E')^2}{2\sigma_E^2}\right] ; \quad (17)$$
$$R_2(L', L) \equiv \frac{1}{\sqrt{2\pi}\sigma_L} \exp\left[\frac{-(L-L')^2}{2\sigma_L^2}\right] .$$

Hence, the event rate now includes the probability that a neutrino of a given L' and E' is detected in the detector with path-length L and energy E. We have

$$N_{\rm bin}^{\alpha,R}(x) = \int_{\rm bin} {\rm d}x \int_{E_{\rm min}} {\rm d}E \int \frac{{\rm d}E'}{E'} R_1(E', E) \int {\rm d}L' R_2(L', L) \mathcal{J} \frac{{\rm d}^2 N^\alpha}{{\rm d}\ln E' {\rm d}\cos\theta'} , \quad (18)$$

where $\mathcal{J}$ is the Jacobean of transformation.

We re-evaluate the event rates and the up/down ratios using this equation, with $\sigma_E = 0.15E'$ and $\sigma_L = 0.15L'$. These are realistic widths obtained by a GEANT analysis of atmospheric neutrino events by both the MONOLITH and the ICAL/INO collaborations. Such a smearing has the effect of accounting for errors in correctly identifying the L/E bin for a given event, and so accounting for bin-to-bin correlations.

We comment in passing on the use of finite widths in L rather than in θ. The smearing in L actually arises because of the uncertainties involved in reconstructing the neutrino direction. Hence, the smearing should be in θ not L. Choosing a resolution in θ rather than in L (or equivalently $\cos\theta$) may give more realistic spreads, especially at large angles where smearing in $\cos\theta$ may underestimate the large variations in L for small changes in θ. This can be seen in Fig. 22. Applying a constant $\Delta L/L$ of 15% corresponds to large angular spreads at small angles where base-lengths are large, while a constant angular width $\Delta\theta$ of 5° leads to larger spreads in baselines at large angles. In this paper, we go with convention [28, 30] and define widths in the base-length L.

In Fig. 23 we show the variation of the up/down events ratio for different Δm^2 values as a function of $\log_{10} L/E$ for $\theta_{23} = 40°, 50°$ when the resolution function is included. The upper panels correspond to smearing in E and θ while the lower panels correspond to smearing in E and L. Here θ_{13} is fixed to 9°. A comparison with the similar Fig. 15, where no resolution functions have been included, shows immediately that the effect of changing the octant of θ_{23} remains roughly the same as before (about 1σ maximum deviation in each bin) while the oscillation pattern itself gets smeared away due to finite resolution functions so that the minima and maxima of the oscillations are not as clearly visible, especially beyond the first minimum. It is seen that the peaks and troughs are better defined when smearing in L rather than θ is used. However, the differences between smearing in L and θ otherwise seem marginal.

Hence the effect of detector resolution is akin to that of increasing θ_{13}, which moves both the minima and maxima of the peaks towards the average value of 1/2. This can be seen in Fig. 24 which shows the variation of the up/down events, with resolution, at $\Delta m^2 = 2.4 \times 10^{-3}$ eV^2, for different values of θ_{13}. It is clear, especially when compared with the corresponding results *without* resolution function in Fig. 17, that the distinction between the curves for different θ_{13} is much reduced. In particular, it is likely that other experiments, for example, Double-CHOOZ, will be able to resolve θ_{13} with better accuracy.

We now go on to study the effect of finite detector resolutions on the extraction of oscillation parameters. We repeat the earlier calculation, where contours of allowed parameter

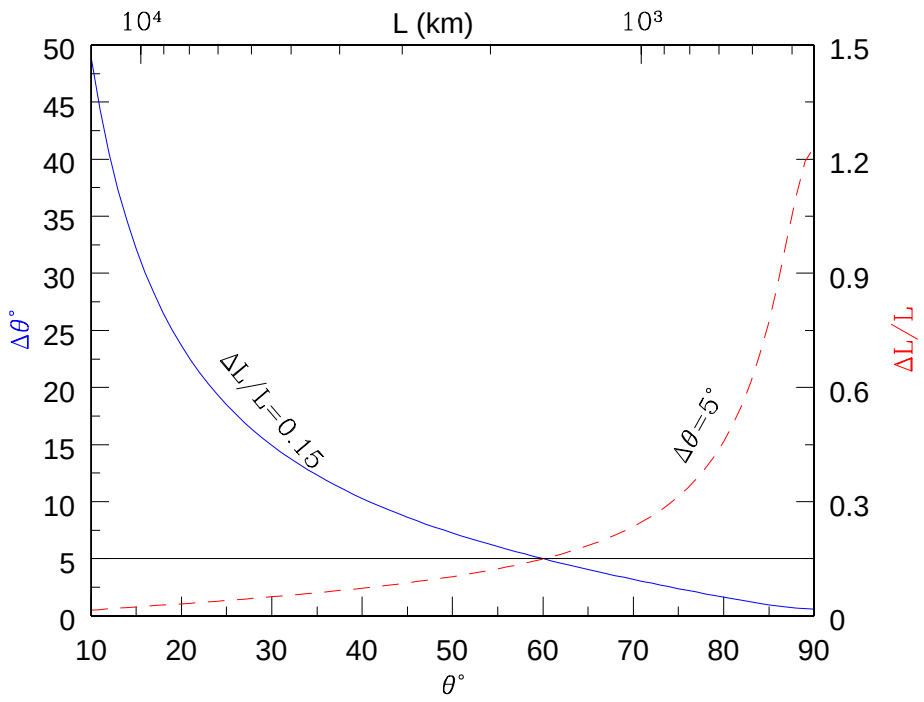

FIG. 22: The figure shows the effective width in nadir angle of a Gaussian smearing in the base-length, with width $\Delta L/L = 0.15$, as the solid line, with axis labelled in $\Delta\theta^\circ$ on the left. It is seen that a constant relative width in base-length corresponds to very small angular smearing in the horizontal direction and large smearing in the vertical direction (small θ or large L). The dashed line conversely shows the smearing in base-length for a constant Gaussian width of $\Delta\theta = 5^\circ$, with the scale in $\Delta L/L$ shown on the axis on the right. It is seen that constant angle and constant relative widths in base-length are complementary to each other in their effects. The x-axis is labelled both in nadir angle $\theta(^\circ)$ and base-length L (km) for convenience.

space were generated for an input data of up/down neutrino and anti-neutrino event rates in fixed L/E bins for a set of input values for $(\theta_{13}, \Delta m^2, \theta_{23})$ and focus, as before, on the octant resolution. We find that for resolution widths $\sigma_E/E = \sigma_L/L = 15\%$ in both E and L, atmospheric neutrino (and anti-neutrino) data accumulated over 1000 kton-years is sufficient to distinguish a non-maximal solution from a maximal solution as well as the octant of θ_{23} for $\theta_{13} \geq 8^\circ$ and $\theta_{23} \leq 39^\circ$ or $\theta_{23} \geq 51^\circ$. However, the inclusion of finite detector resolution severely degrades the errors on the parameters. For instance, the error on Δm^2 is twice as large as that with an ideal detector. This is shown for two values of θ_{13}, $\theta_{13} = 7^\circ, 8^\circ$, for $\theta_{23} = 39^\circ$ ($\sin^2\theta_{23} = 0.4$) and $\Delta m^2 = 2.4 \times 10^{-3}$ eV^2 in Figs. 25 and 26 respectively.

While maximality in θ_{23} can be excluded and the octant distinguished at 95% CL, only deviation from maximality can be established at 99% CL for the smaller $\theta_{13} = 7^\circ$ due to the island around the "wrong octant" solution. It may be mentioned here that a similar analysis has been performed in Ref. [15]. Here a slightly lower neutrino energy was allowed, down to $E = 1$ GeV, although only DIS interactions were considered. Also, the relevant results in this paper focus on discriminating the "right octant" solution from the "wrong octant" one. However, one must exercise caution in such an analysis. It is possible, as is

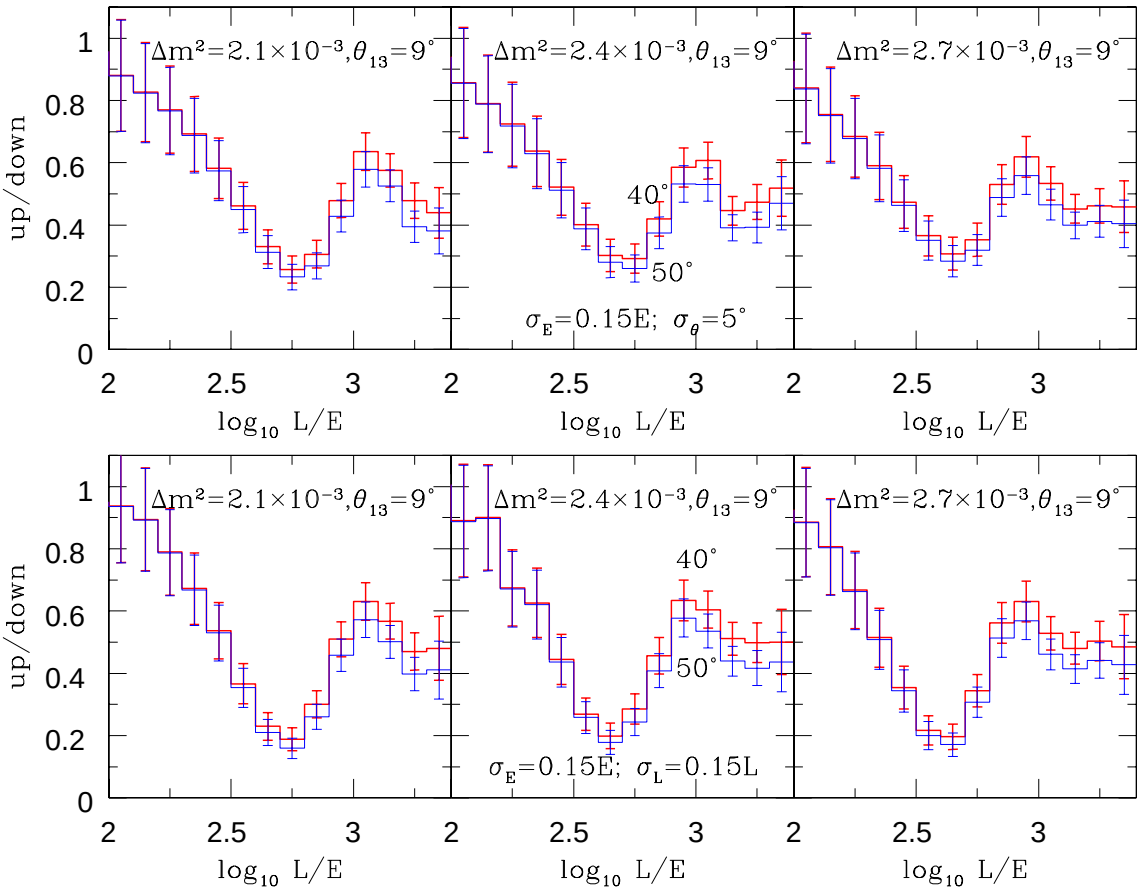

FIG. 23: As in Fig. 15, for $\theta_{13} = 9°$, including finite detector resolutions. Above: smearing in E and θ by Gaussian resolutions with widths $\sigma_E/E = 0.15$ and $\sigma_\theta = 5°$, and Below: smearing in E and L by Gaussian resolutions with widths $\sigma_E/E = \sigma_L/L = 0.15$.

very clearly visible in several of the figures showing allowed parameter space with "wrong octant" islands, that while the exact "wrong octant" solution may be disallowed, a small neighbourhood of this point may still remain allowed. In fact, it is typically seen that the allowed island at 99% CL around the "wrong octant" solution is typically to the right of the central value.

From Figs. 25 and 26 it is seen that a larger θ_{13} is instrumental in suppressing the "wrong octant" solutions but does not shrink the allowed parameter space around the correct θ_{23} value. In fact, the allowed parameter space around $\theta_{23} = 39°$ is virtually the same in both figures. With larger $\theta_{13} = 9°$, it is possible to obtain octant discrimination for larger $\theta_{23} = 40°$, but the issue of maximality can only be settled at little less than 99% CL in this case, as can be seen from Fig. 27. (Of course, if deviation from maximality cannot be established, the octant determination appears to have no meaning. What we mean here is that the allowed parameter space lies mostly in the first octant. The octant mirror of the best-fit point is ruled out, but not the maximal value. We will refer to such solutions as discriminating the octant but not deviations from maximality.) It turns out that both octant and maximality discrimination can be established at 95% CL for values of $\sin^2\theta_{23}$ 15% away from the maximal value. Contrast this with the result (10%) of the previous section when

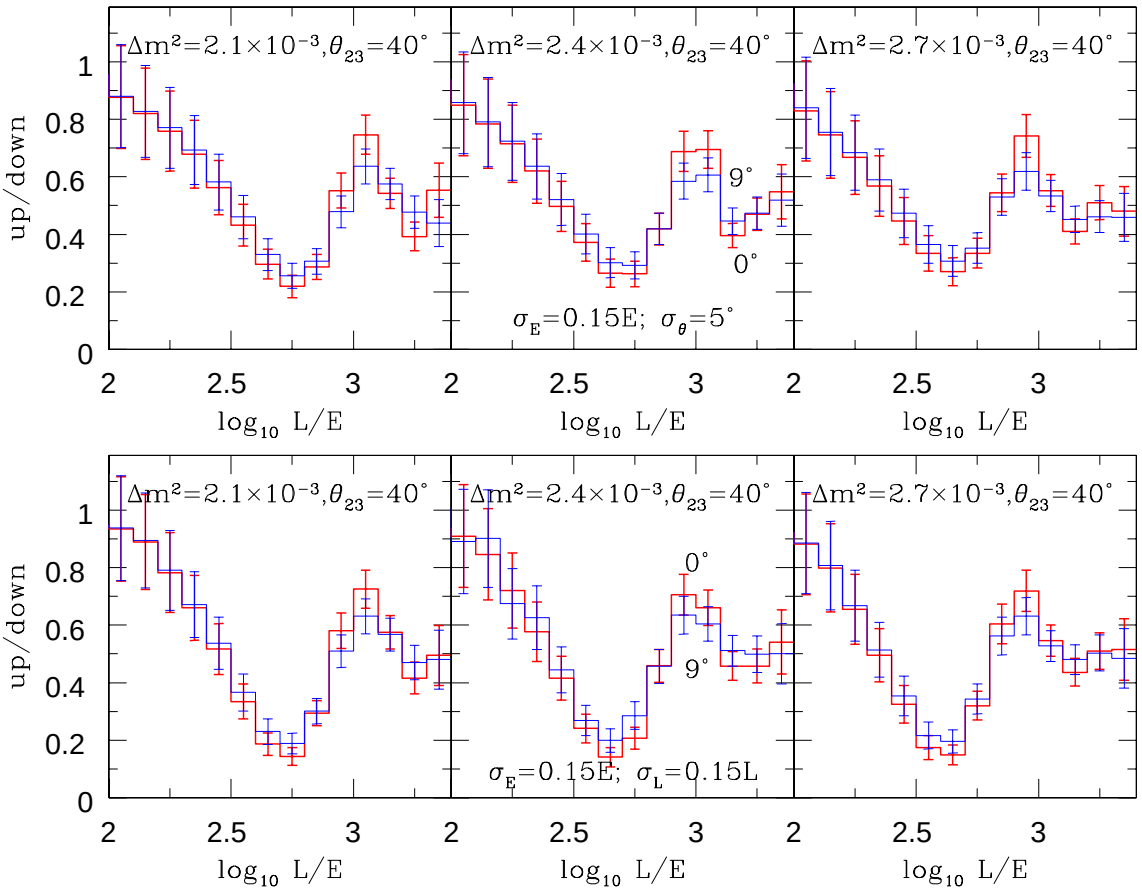

FIG. 24: As in Fig. 17, showing variations with $\theta_{13} = 0, 9°$, where event rates are now calculated including finite detector resolution. For more details see the caption to Fig. 23.

an ideal detector is used.

It is clear that resolution functions worsen the precision with which the magnitude of Δm^2 and θ_{23} can be determined but do not substantially alter the sensitivity to the octant of θ_{23}. That is, $\theta_{13} = 7°$ ($\sin^2\theta_{13} = 0.015$) remains the limit at which matter effects are substantial enough to determine the octant of the (23) mixing angle (as also the mass ordering of the (23) mass eigenstates, as discussed in Ref. [16]), even on including finite resolution functions, while the actual value of the (23) angle which simultaneously allows maximality and octant discrimination at 99% CL level moves marginally from $\theta_{23} = 40°$ in the absence of finite resolution effects, to $\theta_{23} = 39°$ ($\sin^2\theta_{23} \approx 0.4$) at the lower limit of θ_{13}.

We note that the situation is not as clean when the true value of θ_{23} lies in the second octant. The muon survival probability in this case is not as well separated from that for maximal θ_{23}, unlike when θ_{23} is in the first octant (see Fig. 8). Hence, while results for octant discrimination will be symmetric with the case when θ_{23} is in the first octant, the issue of maximality may not be so easily settled. For example, with other parameters as before, and using $\theta_{23} = 51°$, which is the octant mirror of $\theta_{23} = 39°$, the "data" discriminate between the right and wrong octant at 99% CL, but cannot discriminate the true value of θ_{23} from maximality. By going farther away from maximality, for example, at $\theta_{23} = 52.5°$ (and $(\Delta m^2, \theta_{13})$ values of $(2.4 \times 10^{-3}\ \text{eV}^2, 7°)$, as before), we once again have maximality

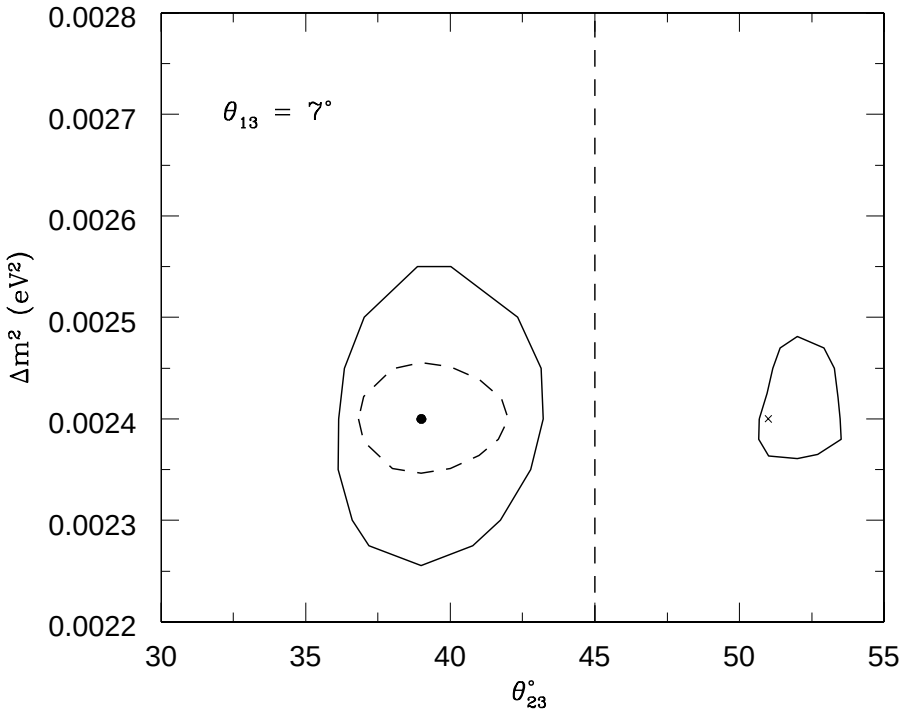

FIG. 25: Allowed parameter space from neutrino and anti-neutrino up/down event rates for an exposure of 1000 kton-years and input parameter values $(\theta_{23}, \theta_{13}) = (39^\circ, 7^\circ)$ for fixed $\Delta m^2 = 2.4 \times 10^{-3}$ eV^2. The 99% CL contours are shown for an ideal detector (dashed lines) and for a detector with finite Gaussian resolutions of widths 15% in E and L. An island of allowed parameter space near the "wrong octant" solution, $\theta_{23} = \pi/2 - \theta_{23}^{\rm input} = 51^\circ$, marked with a a cross, is seen.

discrimination.

E. A note on the inverted hierarchy

The oscillation probabilities and hence up/down events ratio in anti-neutrinos with inverted hierarchy are very similar to those in neutrinos with the normal hierarchy. However, the errors are about two and a half times as large due to the smaller anti-neutrino cross-sections leading to correspondingly smaller event rates. Because of this, a 1000 kton-year exposure is inadequate to address the question of maximality or octant determination of θ_{23}. Both can be determined at 99% CL for an ideal detector for $(\theta_{23}, \theta_{13}) = (37^\circ, 9^\circ)$. When resolution functions are included, only maximality can be established; it is not possible to determine the octant of θ_{23} for any value of θ_{23} allowed by the Super-Kamiokande results (see Table I). In this, our results differ from those of Ref. [15]. By itself, this result is not surprising; otherwise it will imply that 500 kton-year exposure should be adequate for such determinations with normal hierarchy, which is not the case.

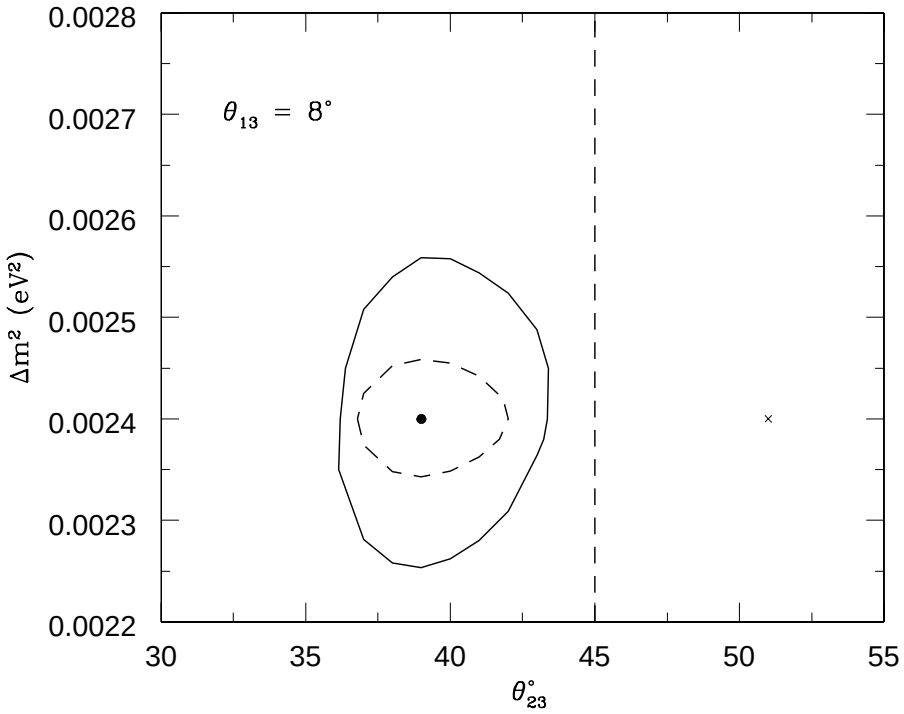

FIG. 26: As in Fig. 25 for $\theta_{13} = 8°$. There is no allowed parameter space near the "wrong octant" solution, $\theta_{23} = \pi/2 - \theta_{23}^{\rm input} = 51°$, marked with a cross in the figure.

V. DISCUSSION AND SUMMARY

Neutrino oscillation studies are now moving to the precision determination of oscillation parameters. The most interesting questions in this field today centre around the issue of whether the (13) mixing angle is different from zero and its implications. The impact of this fundamental parameter and others were analysed in the first part of this paper. In particular we find:

- θ_{13} sensitivity: With θ_{13} nonzero, for energies beyond 3 GeV, there is a sharp discontinuity in the survival as well as conversion probabilities, $P_{\mu\mu}$ and $P_{e\mu}$, at the mantle-core boundary at nadir angle 33°. (See Fig. 2 and 3). For small path lengths (within the mantle) increasing θ_{13} simply decreases (increases) the amplitude of $P_{\mu\mu}$ at the maxima (minima) without significantly altering the oscillation period.

  However, as the paths cross the mantle-core boundary and propagate within the core, the matter effects significantly modify the period of oscillations as well, for both the survival and conversion probabilities. In particular, the jump in $P_{e\mu}$ at the mantle-core boundary becomes larger and more visible with increasing θ_{13}. (See Fig. 3). This important feature can be used with long baseline neutrinos for Earth tomography studies.

- Δm^2 sensitivity: A variation in this parameter changes the period of oscillations, even in the absence of matter effects. For non-zero θ_{13}, with the matter effects turned on, there are dramatic changes in the probabilities, as again both the periods and

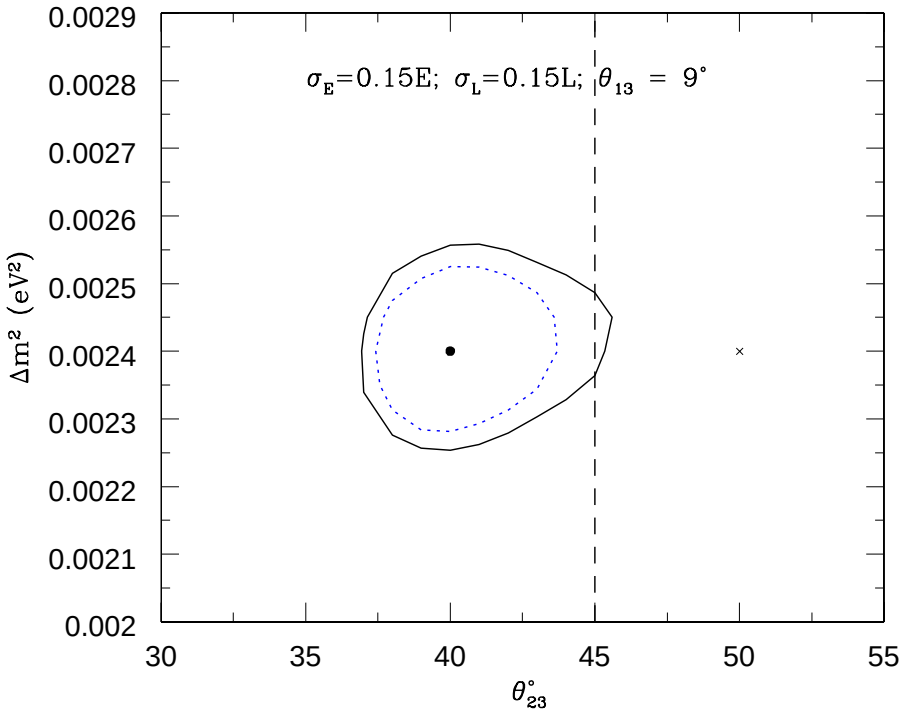

FIG. 27: Allowed parameter space in $(\theta_{23}, \Delta m^2)$ variables. Input used was $(40^\circ, 2.4 \times 10^{-3}$ eV$^2)$, for $\theta_{13} = 9^\circ$, where the up/down ratio was analysed using finite resolution functions in E and L of widths 15% each. Shown are the allowed 95% and 99% CL contours. While octant discrimination is possible at 99% CL, the issue of maximality can only be settled at somewhat better than 95% CL.

amplitudes are dramatically altered, especially at around 5 GeV. (See Fig. 5). At around 2 GeV, a substantial $P_{e\mu}$ at small nadir angles indicates a rather small Δm^2, $\Delta m^2 \lesssim 2 \times 10^{-3}$ eV^2. (See Fig. 7).

- θ_{23} sensitivity: For θ_{13} nonzero, we note that as θ_{23} increases from the first octant through to the second octant, the survival probability systematically decreases for most nadir angles in the energy range 5–10 GeV. (See Fig. 8). However, the conversion probability, $P_{e\mu}$ systematically increases as θ_{23} increases at all nadir angles and all energies. This is not very significant for atmospheric neutrinos, but can be studied separately with long baseline neutrinos.

Finally, the probabilities are sensitive to variations in the PREM profile (within allowed limits) as also the CP phase. However, these dependences are rather small and insignificant and are unlikely to be measured with atmospheric neutrino studies of the type discussed here. The results discussed for CP phase in this paper can therefore be seen only with long baseline neutrinos when all other parameters are presumably known to good precision.

The probabilities $P_{\mu\mu}, P_{e\mu}$ are then used to analyse the atmospheric muon neutrino events to determine the deviation from maximality and/or the octant of the (23) mixing angle θ_{23}. Such dependence arises purely from matter effects as the neutrinos propagate through Earth. Since matter effects are different in the case of neutrinos and anti-neutrinos, we assume a

detector with charge discrimination capability, such as the proposed ICAL/INO detector, to heighten the sensitivity to such matter-dependent effects. Moreover, all matter terms are proportional to $\sin^2\theta_{13}$ so we assume that this (13) mixing angle is different from zero.

We study the up/down events ratios, where by up (down)-neutrinos, we mean neutrinos arriving at the detector from below (above), so their nadir angles range from 0–90° (90–180°). Analysis of ratios of events rather than events themselves significantly reduces errors from overall normalisation of fluxes and cross-sections; the former can be as large as 30% and the latter around 10%. Smearing in energy E and base-length L by use of Gaussian functions is used to simulate finite detector resolutions. Typical relative widths of 15% are used for both energy and base-length. The allowed parameter space obtained on fitting up/down neutrino and anti-neutrino events ratios in any two of $(\Delta m^2, \theta_{23}, \theta_{13})$ is considered.

Since the up/down events ratio has very different dependence on θ_{23} and θ_{13}, in principle, they can be simultaneously determined from such studies. The proposed detectors such as ICAL/INO with charge identification capability may be in principle suitable for determination of these parameters. In practice, however, these detectors are not well suited for precision determination of θ_{13} with atmospheric neutrinos. A precise measurement of this parameter is likely to be made, for instance, by the Double-CHOOZ experiment.

We summarise below our observations on the simultaneous determination of $|\Delta m^2|$ and θ_{23} from an analysis of the event rates at these detectors with focus on the determination of θ_{23}. We distinguish three scenarios. The best case is when both deviation of θ_{23} from maximality as well as its octant can be established. In some cases, a maximal value of θ_{23} is disallowed, so deviations from maximality can be established but the octant discrimination may not be possible. The third is where the *best-fit* value lies in one of the octants and the region in parameter space around the mirror to the best-fit value in the other octant is ruled out at the precision under consideration; however, the maximal value is not ruled out at this precision. In such a case, the allowed parameter space still lies mostly in one octant and hence we consider that we have octant but not maximality discrimination.

- If θ_{13} is known precisely in the near future, as is likely from Double-CHOOZ, then in the energy range $E = 5$–10 GeV, where matter effects are largest, the data from ICAL/INO will be able to study deviations of θ_{23} from maximality as well as determine the octant of this angle, provided $\theta_{13} \geq 7^\circ$.

- It must be emphasised that the octant discrimination is more easily done than establishing deviation from maximality for larger θ_{13} and the reverse is true for smaller θ_{13} when islands of allowed parameter space begin to appear near the "wrong octant" solution. Also, values of θ_{23} in the first octant are more easily distinguished from maximality than those in the second octant. This result is in contrast to those obtained in Ref. [15].

- In particular, deviations from maximality and octant discrimination to 99% CL can be obtained if $\sin^2\theta_{23} \leq 0.4$ and $\sin^2\theta_{13} \geq 0.015$. These studies used standard Gaussian resolution functions with widths $\delta L/L = \delta E/E = 15\%$ to smear the events. Similarly, we must have $\sin^2\theta_{23} \geq 0.63$ for corresponding results in the second octant.

- In an earlier paper[16], it was also shown that the same processes are also eminently suited to determine the (23) mass ordering. Both these determinations need large exposures of roughly 1000 kton-years as well as, crucially, the charge discrimination.

- As discussed in [16], the issue of determining the (23) mass ordering and hence establishing the neutrino mass hierarchy is best done using the difference asymmetry defined in Eq. 15 which is the *difference* of the up/down events ratios with neutrinos and anti neutrinos. For the octant discrimination that is the crux of this paper, the relevant observable is in fact the *sum* of these two ratios.

- The same experiment can therefore study both these questions, while requiring large exposures, 1000 kton-years, in both cases. Hence, studies of neutrino oscillations with atmospheric neutrinos, while being difficult, are probably the only source of precision measurements, at least until very large megaton detectors and/or neutrino factories become a reality.

Even so, it is important to point out that the determination of the hierarchy is likely to be relatively easier than the octant determination. This is because, as seen from Fig. 16, the octant effect rides on the hierarchy issue as a sub-dominant effect.

Another way to see this is that the octant determination is dominated by the (anti) neutrino events ratio in the (inverted) normal hierarchy, which are the relevant sectors where matter effects dominate. Since the statistics is smaller by half for anti-neutrinos for the same exposure, the significance of the results deteriorates in the case of inverted hierarchy.

The bulk of the results presented in this paper therefore pertain to the normal mass hierarchy. Results of similar significance can only be established with the inverted mass hierarchy if the exposure is at least twice that for normal hierarchy. Hence, such detectors, with exposures of 1000 kton-year or so, may be able to settle the issue of mass hierarchy but, if the ordering is inverted, the issue of maximality of θ_{23} may remain an open question.

Acknowledgements: We are grateful to Dave Casper for making the NUANCE software freely available, and answering a long list of questions on its use. The work of N.S. was partially supported by the Department of Science and Technology, India.

VI. APPENDIX

One of the earliest analytical methods for the calculation of oscillation probabilities with variable matter density is in Ref. [20]. The oscillation probability was derived assuming matter to be made up of a series of slabs through which neutrinos and anti-neutrinos propagate. Each slab has smoothly varying density, but the density itself has discrete jumps at the junction of adjacent slabs. In a recent paper, Akhmedov et al. [21], have provided an excellent collection of approximate analytic formulae for the neutrino oscillation probabilities. Exact analytical formulae have also been derived in the case of vacuum [22] and for matter with constant density slabs [23]. Though complicated, exact analytic formulae have been derived for non-uniform density with linear [24] and exponentially [25] varying density. Approximate analytic formulae with varying assumptions have been derived in a number of papers [26].

Here, we use a standard Runge-Kutta solver to numerically propagate the neutrinos through Earth's matter, using the PREM Earth density profile for a spherical equivalent Earth with radius $R_E = 6371$ km. We outline some details about the numerical calculation. We also highlight how results from an algorithm using constant density slabs differ from those with the PREM profile. Our technique is to numerically evolve the flavour eigenstates

using the equation,

$$i\frac{\mathrm{d}}{\mathrm{d}t}\left[\nu_\alpha\right] = \frac{1}{2E}\left(UM^2U^\dagger + \mathcal{A}\right)\left[\nu_\alpha\right] \ , \tag{6}$$

where $\mathcal{A}$ is the diagonal matrix, $\mathrm{diag}(A,0,0)$ and $[\nu_\alpha]$ denotes the vector of eigenstates, ν_α, $\alpha = e,\mu,\tau$. As usual, U is the MNS mixing matrix defined in Eq. 2, M^2 is the mass-squared matrix with the diagonal piece proportional to m_1^2 removed: $M^2 = \mathrm{diag}(0,\delta_{21},\delta_{31})$. Note that in a constant density slab approximation, the mass eigenstates are propagated, including the "sudden" jumps across the density discontinuities.

As mentioned in the text, the chief difference between the constant density approximation and the PREM profile lies in the resonance effects. This can be seen from Fig. 28 where the results of using the PREM profile in our calculations, and the NUANCE [17] result for the same parameters, using constant density slabs, is shown. Here we have set the parameters δ_{21}, Δm^2 (normal hierarchy), θ_{21} and θ_{23} to their best-fit values as given in Table I and set the CP phase to zero. We use $\theta_{13} = 9°$. For a low value of $E = 2.51$ GeV, where resonance occurs in the core, the constant density slab of NUANCE does not show resonance since the precise density value needed for resonance does not occur. Of course, matter effects are present and are large; however, this difference causes the two curves for the neutrino survival probability to begin to separate in this region, as can be seen from the top left panel of the figure. It is seen that the anti-neutrino probabilities, which are relatively insensitive to matter effects in the normal hierarchy, however, match exactly.

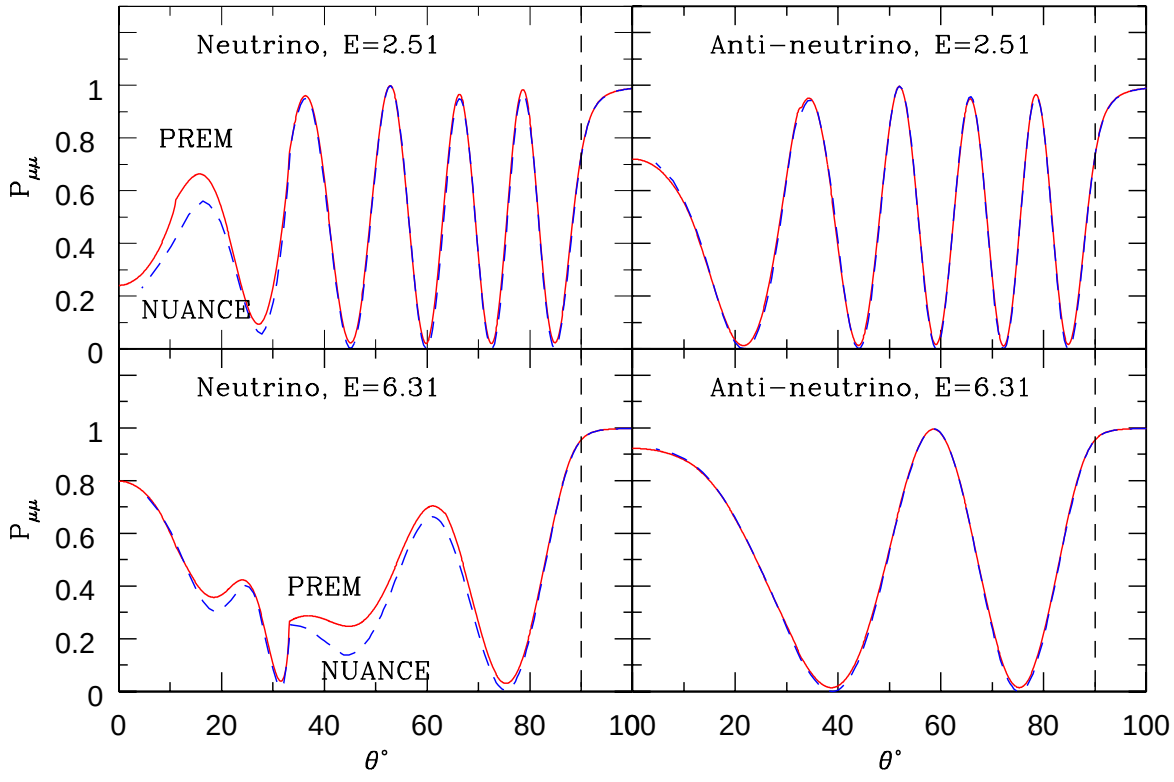

FIG. 28: The muon neutrino and anti-neutrino survival probability as a function of nadir angle for different energies. Shown are the results from an exact numerical method using the PREM Earth density profile (solid lines) and a constant density slab model from NUANCE [17].

At larger energies, $E = 6.31$, the "missed" resonance occurs in the mantle itself. Hence, deviations between the two curves are seen at almost all zenith angles. The difference can be up to 10–15%. Note also that the prominent effect of core-crossing, which occurs at 33°, can be seen clearly in both curves. Again, the anti-neutrino probabilities match.

We have also checked that, by taking smaller and smaller slabs, and approximating the PREM profile as closely as possible, the results from the constant density slab approach those using the exact Runge-Kutta solver with PREM profile. However, the resultant increase in number of slabs is quite large.

[1] S.N. Ahmed et al. (SNO Collaboration), Phys. Rev. Lett. **92**, 181301 (2004) [ArXiv:nucl-ex/0309004]; Q.R. Ahmad, et al. (SNO Collaboration), Phys. Rev. Lett. **89**, 011302 (2002); Phys. Rev. Lett. **89**, 0113010 (2002), Phys. Rev. Lett. **87**, 071301 (2001); S. Fukuda, et al. (Super-Kamiokande Collaboration), Phys. Lett. **B 539**, 179 (2002), Phys. Rev. Lett. **86**, 5656 (2001); Phys. Rev. Lett. **86**, 5651 (2001); Fukuda, Y. et al. (Super-Kamiokande Collaboration), Phys. Rev. Lett. **82**, 2430 (1999); Phys. Rev. Lett. **82**, 1810 (1999); Phys. Rev. Lett. **81**, 1158 (1998); W. Hampel, et al. (GALLEX Collaboration), Phys. Lett. **B 447**, 127 (1999); J.N.Abdurashitov, et al. (SAGE Collaboration), Phys. Rev. Lett. **83**, 4686 (1999); K.S. Hirata, et al. (Kamiokande-II Collaboration), Phys. Rev. **D 44**, 2241 (1991); R. Davis, (Homestake) Prog. Part. Nucl. Phys. **32**, 13 (1994).

[2] Y.Fukuda, et al.(Super-Kamiokande Collaboration), Phys. Rev. Lett. **81**, 1562 (1998); G. Giacomelli et al. (MACRO Collaboration) Nucl. Phys. Proc. Suppl. **145** 116 (2005).

[3] K. Eguchi et al. (KamLAND Collaboration), Phys. Rev. Lett. **90**, 021802 (2003); Apollonio, M. et al. (CHOOZ Collaboration), Eur. Phys. J. **C 27**, 331 (2003).

[4] M.H. Ahn, et al. (K2K Collaboration), Phys. Rev. Lett. **90**, 041801 (2003).

[5] Y. Ashie et al. (Super-Kamiokande Collaboration), Phys. Rev. Lett. **93**, 101801 (2004); M. Ishitsuka (Super-Kamiokande Collaboration), NOON2004, The 5th Workshop on "Neutrino Oscillations and their Origin", 11-15 February 2004, Tokyo, Japan.

[6] B. Pontecorvo, J. Exp. Theor. Phys. **33**, 549 (1957); Sov. Phys. JETP, **6**, 429 (1958).

[7] Z. Maki, M. Nakagawa and S. Sakata, Prog. Theor. Phys. **28**, 870 (1962).

[8] J. Bernabeu, S. Palomares-Ruiz and S. T. Petcov, Nucl. Phys. **B 666**, 255 (2003); S. Palomares-Ruiz and S. T. Petcov, Nucl. Phys. **B 712**, 392 (2005).

[9] G. L. Fogli, E. Lisi, D. Montanino and G. Scioscia, Phys. Rev. **D 55**, 4385 (1997).

[10] P. Huber, M. Maltoni and T. Schwetz, Phys. Rev. **D 71**, 053006 (2005).

[11] E. K. Akhmedov et al., Nucl. Phys. **B 542**, 3 (1999).

[12] T. Tabarelli de Fatis, Eur. Phys. J. **C 24**, 43 (2002).

[13] R. Gandhi et al., Phys. Rev. **D 73**, 053001 (2006) [ArXiv:hep-ph/0411252]; R. Gandhi et al., [ArXiv:hep-ph/0506145].

[14] Debajyoti Choudhury and Anindya Datta, JHEP **0507**, 058 (2005) [ArXiv:hep-ph/0410266].

[15] S. Choubey and P. Roy, Phys. Rev. D **73**, 013006 (2006) [arXiv:hep-ph/0509197].

[16] D. Indumathi and M.V.N. Murthy, Phys. Rev. **D 71**, 013001 (2005) [ArXiv:hep-ph/0407336].

[17] NUANCE Neutrino Generator, D. Casper, Nucl. Phys. Proc. Suppl. **112**, 161 (2002); see http://www.ps.uci.edu/∼nuint/nuance/default.htm.

[18] M.C. Gonzalez-Garcia and Y. Nir, Rev. Mod. Phys. **75**, 345 (2003) [ArXiv: hep-ph/020205].

[19] G.L. Fogli, E. Lisi, A. Marrone, A. Palazzo, ArXiv:hep-ph/0506083, to appear in Progress in Particle and Nuclear Physics, 2006.

[20] Mohan Narayan, G. Rajasekaran, Rahul Sinha, Mod. Phys. Lett. **A 13**, 1915 (1998); see also G. Rajasekaran, Pramana **55**, 19 (2000) (Plenary talk given at Workshop in High Energy Particle Physics-6, Chennai, India).

[21] Evgeny K. Akhmedov, Robert Johansson, Manfred Lindner, Tommy Ohlsson and Thomas Schwetz, JHEP **0404**, 78 (2004).

[22] S.M. Bilenky and S.T. Petcov, Rev. Mod. Phys. **59**, 671 (1987).

[23] V.D. Barger, S. Pakvasa, K. Whisnant, and R.J.N. Phillips, Phys. Rev. **D 22** 2718 (1980); for a review see ref.[18].
[24] H. Lehmann, P. Osland and T.T. Wu, Commun. Math. Phys. **219**, 77 (2001).
[25] P. Osland and T.T. Wu, Phys. Rev. D**62**, 013008 (2000).
[26] A. Bueno, M. Campanelli and A. Rubbia, Nucl. Phys. **B 589**, 577 (2000).
[27] A.M. Dziewonski and D.L. Anderson, Preliminary reference Earth model (PREM), Phys. Earth Plan. Int. **25**, 297 (1981).
[28] N.Y. Agafonova et al., The MONOLITH proposal, LNGS P26/2000, CERN/SPSC 2000-031, August 2000 (http://castore.mib.infn.it/∼monolith/proposal/).
[29] A. Para, Acta Phys. Polon. **B 31**, 1313 (2000) [ArXiv:hep-ph/0005012]; C. Andreopoulos, P. Stamoulis and G. Tzanakos, NuMI-Note-ATM_NU-990, UA/ Phys/ HEP/ 11-05-2003 (http://www-numi.fnal.gov/).
[30] D. Indumathi (INO Collaboration), Proc. 29th International Conf. on Cosmic Rays, ICRC, Pune, **Vol 10**, 199 (2005); (http://www.imsc.res.in/∼ino).
[31] W. Winter, Phys. Rev. **D 72** (2005) 037302; T. Ota, J. Phys. **G 29**, 1869 (2003).
[32] P. Huber and W. Winter, Phys. Rev. **D 68** 037301 (2003), arXiv: hep-ph/0301257.
[33] Patrick Huber, Manfred Lindner, Walter Winter, JHEP 0505 (2005) 020 [ArXiv: hep-ph/0412199].
[34] P. Picchi and F. Pietropaolo, ICGF RAP. INT. 344/1997, Torino 1997 (CERN preprint SCAN-9710037).
[35] M. Honda, T. Kajita, K. Kasahara, S. Midorikawa, Phys. Rev. **D 64**, 053011 (2001).
[36] F. Ardellier *et al.*, *Letter of intent for double-CHOOZ: A search for the mixing angle theta(13),* arXiv:hep-ex/0405032. See also http://doublechooz.in2p3.fr.